International Journal of Biological Macromolecules 229 (2023) 974–993

Contents lists available at ScienceDirect

International Journal of Biological Macromolecules

journal homepage: www.elsevier.com/locate/ijbiomac

Review

Metal ion chelation of poly(aspartic acid): From scale inhibition to therapeutic potentials

Hossein Adelnia [a,b], Fariba Sirous [d], Idriss Blakey [b], Hang Thu Ta [a,b,c,*]

[a] Queensland Micro-and Nanotechnology Centre, Griffith University, Nathan, Queensland 4111, Australia
[b] Australian Institute for Bioengineering and Nanotechnology, University of Queensland, St Lucia, Queensland 4072, Australia
[c] Bioscience Discipline, School of Environment and Science, Griffith University, Nathan, Queensland 4111, Australia
[d] Department of Chemistry, Isfahan University of Technology, Isfahan 84156-83111, Iran

ARTICLE INFO

Keywords:
Poly(aspartic acid)
Chelation
Metal ions

ABSTRACT

Poly(aspartic acid) (PASP) is a biodegradable, biocompatible water-soluble synthetic anionic polypeptide. PASP has shown a strong affinity and thus robust complexation with heavy and alkaline earth metal ions, from which several applications are currently benefiting, and several more could also originate. This paper discusses different areas where the ion chelation ability of PASP has thus far been exploited. Due to its calcium chelation ability, PASP prevents precipitation of calcium salts and hence is widely used as an effective scale inhibitor in industry. Due to potassium chelation, PASP prevents precipitation of potassium tartrate and is employed as an efficient and edible stabilizer for wine preservation. Due to iron chelation, PASP inhibits corrosion of steel surfaces in harsh environments. Due to chelation, PASP can also enhance stability of various colloidal systems that contain metal ions. The chelation ability of PASP alleviated the toxicity of heavy metals in Zebrafish, inhibited the formation of kidney stones and dissolved calcium phosphate which is the main mineral of the calcified vasculature. These findings and beyond, along with the biocompatibility and biodegradability of the polymer could direct future investigations towards chelation therapy by PASP and other novel and undiscovered areas where metal ions play a key role.

1. Introduction

Poly(aspartic acid) (PASP) is a biodegradable, biocompatible water-soluble anionic polypeptide [1–7]. A great deal of attention has recently been paid to this synthetic polyacid as well as its amide derivatives (i.e., polyaspartiamide) specifically for biomedical applications due to their facile synthesis, modification, and the above-mentioned features [1,2]. PASP can also be crosslinked with a variety of crosslinking agents to form hydrogels, further extending its uses in various areas [8]. This includes but not limited to tissue engineering, drug delivery, and medical utilization, where the design and development of (super)absorbents remain to be of great interest [9].

A strong affinity with heavy (e.g., Cd, Fe, Co, Cu, Ni) and alkaline earth metal cations (e.g., Ca, Sr, Ba) is regarded as one of the most important features of PASP. Such affinity results in the formation of strong complexes with these ions which is referred to as chelation. Ion chelation of PASP originates from the unique positions of the two adjacent carboxylic acid groups as well as its lone pair electrons from nitrogen in the backbone (CONH) [10]. Such a configuration enables effective ion entrapment for the formation of water-soluble PASP-metal ion complexes. The specific chemical structure of PASP also differentiates it from other anionic natural polymers such as alginate, carboxymethyl cellulose, xanthan, hyaluronic acid, carrageenan, as well as synthetic ones such as poly (acrylic acid) [11,12].

Such robust complexation with metal ions could be exploited in a variety of areas. For instance, it can prevent undesirable mineral precipitation/deposition which occurs as a result of supersaturation of ions, causing severe not only in various industrial equipment and machinery but in the human body [13,14]. PASP has also been employed for stabilization of particles [15], wine preservation [16] and water purification [17] (Fig. 1). Metal ion chelation of PASP can also be exploited for the development of fertilizers containing nitrogen, phosphorous, calcium, potassium, etc., to enhance crop growth and soil quality [18]. Furthermore, PASP and its derivatives, thanks to their hydrophilicity,

* Corresponding author at: School of Environment and Science and Queensland Micro and Nanotechnology, Griffith University, Nathan Campus, Brisbane, QLD 4111, Australia.
E-mail address: h.ta@griffith.edu.au (H.T. Ta).

https://doi.org/10.1016/j.ijbiomac.2022.12.256
Received 1 September 2022; Received in revised form 21 December 2022; Accepted 22 December 2022
Available online 27 December 2022

can also be used as moisturizers in cosmetics and various skin care products [19].

Various aspects of PASP in terms of synthesis, modification, biocompatibility, biodegradation, and biomedical applications have recently been reviewed thoroughly [20–24]. Preparation and applications of PASP hydrogels were also discussed by us recently [8,20]. However, little attention has been paid to the use of PASP and its derivatives as a chelating agent. Thus, this paper comprehensively discusses the chelation ability of PASP as a potent, biocompatible, and biodegradable metal-binding polymer. The complexation abilities of PASP have been used in a wide range of areas as mentioned above. It is envisioned that in the future, further innovative applications are designed, examined, and launched by this polymer. The search strategy for this review employs Google Scholar with no date limitation and the following keywords poly(aspartic acid), chelation, complexation, and metal ion. For each section of the review, its title was added to the keywords to narrow results, thereby retrieving articles and patents that are most relevant to the topic.

2. Synthesis of PASP

As mentioned, synthesis and modification of PASP have been discussed and reviewed thoroughly previously [8,20–22]. Briefly, PASP is conventionally synthesized by thermal polycondensation reaction of aspartic acid, which yields polysuccinimide (PSI) [referred to as poly (anhydroaspartic acid)] as intermediate/precursor (Fig. 2) [20]. The alkali hydrolysis of the latter yields PASP. However, at large scales, PASP is prepared from PSI synthesized by polymerization of maleic anhydride and ammonia because they are inexpensive and easily available raw materials, compared to aspartic acid [25]. The commercially synthesized PASP usually has a low molecular weight (3 to 10 kDa). The product of alkali hydrolysis of PSI is PASP with both α- and β amide linkage as succinimide ring can be opened through either of the carbonyl groups. It was shown that regardless of the reaction conditions used for PSI synthesis, the ratio of α to β amide linkage is 1 to 3 [26]. In another study, Low et al. obtained the α to β of 0.3 to 0.7 by ^{13}C NMR [27].

3. Effect of PASP characteristics on chelation

The ion chelation ability of PASP could be affected by a variety of factors such as type of chirality, type of amide linkage in the polymer backbone, polymer molecular weight, pH of the medium where ions are present, and the presence of other ions. These factors are briefly discussed below. As summarized in Table 1, calcium chelation to PASP is not strongly influenced by the chirality (L or D type), while the α amide linkage showed higher chelation compared to the β, and the combination of α and β [3]. It has been postulated that the longer distance of COOH groups from the polymer backbone in α-PASP compared to that in β-PASP results in a more effective chelation of calcium ions. Furthermore, molecular simulation of the interactions between calcium carbonate ($CaCO_3$) and PASP with different amide linkage types showed the binding energy in the order of α-PASP > α + β- PASP > β-PASP [28]. α-PASP was also found to have the highest ability for conformational changes when mixed with $CaCO_3$ [28]. Nevertheless, availability and relatively simple synthesis of PASP through thermal step-growth polymerization, which typically yields α to β of 0.3 to 0.7, makes them widely used both in academia and industry, compared to other types of PASP with specific amide linkage or chirality [29].

The molecular weight of PASP can also influence ion chelation. By increasing the chain length from monomer to dimer, trimer, and pentamer, the chelation ability increased (Table 1) [3]. Compared to pentamers, the polymers showed higher chelation ability. These results confirmed the importance of polyvalency of PASP in chelation, as demonstrated in other studies too [30–32]. Nevertheless, recent reports have shown that very high molecular weights are not in favor of chelation when compared to moderate molecular weight [33,34]. For example, PASP with M_w of 3 kDa had a faster dissolution rate of calcite

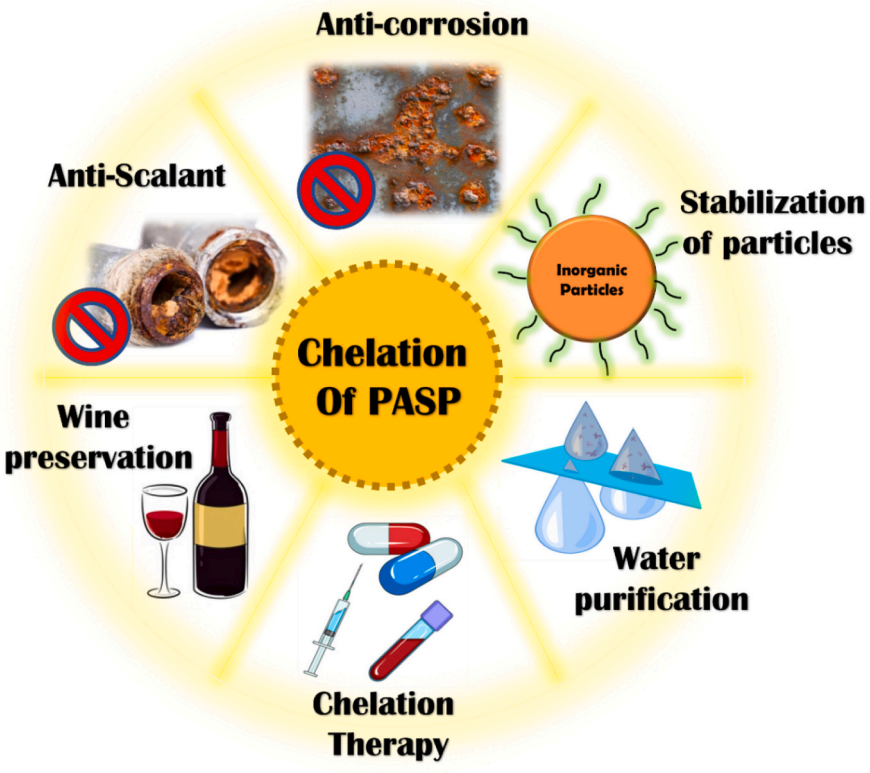

Fig. 1. Ion chelation ability of poly(aspartic acid) exploited in different applications.

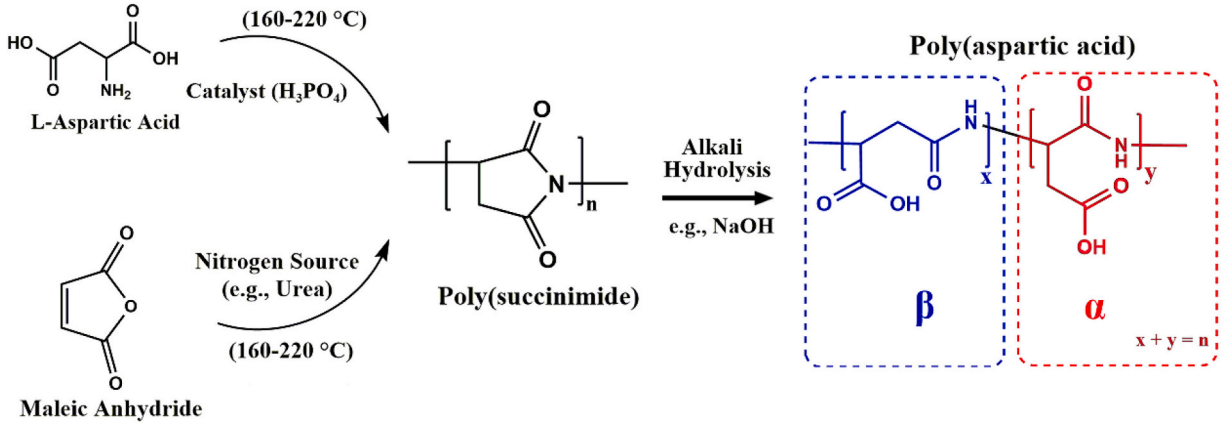

Fig. 2. Synthesis of PASP. Two commonly used polymerization pathways for synthesis of poly(succinimide) (PSI) as the precursor through hydrolysis of which PASP is prepared. The first pathway is step-growth polymerization of aspartic acid as the monomer and phosphoric acid as a catalyst. The second one is based on reaction of maleic anhydride with a nitrogen source (e.g., ammonia), followed by the polymerization of the product which is maleamic acid at high temperatures [20].

Table 1
Effect of the polymer structure on the calcium chelation ability of aspartic acid monomer, oligomers and polymers [3].

Chelator	Mw (Mw/Mn)	Ca^{2+}ion chelation (gram of calcium ion/100 g of the chelator)
L-aspartic acid	–	0.85
L-aspartic acid dimer	–	3.60
L-aspartic acid trimer	–	3.57
L-aspartic acid tetramer	–	5.05
L-aspartic acid pentamer	–	4.95
Poly(α-L-aspartic acid)	31 kDa (1.5)	6.50
Poly(α-D-aspartic acid)	31 kDa (1.5)	6.50
Poly(α,β-D,L-aspartic acid)	34 kDa (1.4)	6.00
Poly(α,β-D,L-aspartic acid)	80 kDa (2.2)	5.40
Poly(β-L-aspartic acid)	64.3 kDa (1.9)	5.70

when compared to PASP with M_w of 10 kDa [33]. The inverse relationship of molecular weight with chelation ability was attributed to a higher level of freedom in conformational change for small size macromolecules. Such a relationship in PASP agrees with results for other polyelectrolytes such as polyacrylic acid [33,34].

As a polyelectrolyte, conformation and chelation of PASP chains strongly depends on the pH of the medium. This is in contrast to non-ionic polymers such as polyvinyl alcohol and polyethylene glycol where the chain conformation is not affected by pH [35,36]. Similar to other anionic polymers (i.e., polyacids), PASP adopts extended and collapsed chain conformation as a result of deprotonation and protonation of carboxylic acid groups, under alkaline and acidic conditions, respectively [37]. Under the alkaline conditions, protons of COOH groups are easily dissociated and the negative charges along the chain repel each other, extending the conformation. The chain conformation of PASP and its transition from the coil to helix and vice versa were studied by voltammetric method in the presence of Zn ions [38]. It was shown that zinc ions coordinate with the dissociated COO-groups in the helical part of PASP, leading to the aggregation of polypeptide strands.

For cation chelation, the polymer should be in ionized form, not in protonated form so that the metal ions can chelate to the carboxylate anions. Thus, one can conclude that for PASP to be efficacious, the medium should not be acidic. Wu et al. [39] modeled PASP ionization and found 4 pK_a values of 2.3, 3.6, 4.1, and 5.2 for the polymer. Successive ionization of the 4 hypothetical aspartyl groups were shown with complete protonation and deprotonation occurring at pH values around 1, and 7, respectively (Fig. 3a). The calcium chelation was in a good agreement with the ionization behavior of PASP, where all calcium ions in the solution were found free at pH < 2 and complexed at pH > 6.5 (Fig. 3b). It is important to note that similar to other polyelectrolytes, the conformation of PASP could be affected by ionic strength. The higher the ionic strength, the higher the charge screening which subsequently results in collapsed chain conformation, and polymer precipitation under severe conditions [40,41]. Therefore, reduced chelation efficacy is likely at high ionic strength [42].

PASP with 50 repeat units was immobilized on pore glass, packed in a glass column, and used for the sequestering of metal ions. The ion uptake capability and selectivity were determined from the acid strip and breakthrough curves in the order of $Fe^{3+} > Al^{3+} > Cu^{2+} > La^{3+} > Pb^{2+} > Cd^{2+} > Ni^{2+} > Co^{2+} > Mn^{2+} > Ca^{2+} > Na^{+}$ [43]. According to the results obtained by Gutierrez et al. [43] (listed in Table 2), PASP's selectivity is consistent with that of negatively charged oxygen donors such as carboxylic acids under biological conditions [44]. In other words, such hard donors bind to hard metal ions (e.g., Cu^{2+} and La^{3+}) more efficiently. However, PASP showed a good affinity with soft metal ions such as Pb^{2+} and Cd^{2+}, as well. This high affinity can be explained by the interaction of the lone pair of PASP (from peptide linkage: –CO–N–R) with the soft metal ions [45]. Malachowski et al. [46] immobilized PASP and PGA on the controlled pore glass and tested the absorption of different metal ions at pH 7. The results showed that both polymers have comparable binding abilities in the following order; $Cu^{2+} > Pb^{2+} > Cd^{2+} \approx Ni^{2+} > Co^{2+} > Mn^{2+} > Na^{+}$. As seen, the trend is similar to the above-mentioned studies. Mixed metal binding also revealed that the polymer selectivity towards Cu^{2+} and Pb^{2+} rather than towards Cd^{2+} and Ni^{2+} such that the former ions displaced the latter ions bound to the polymers. It was reported that aside from the peptide chain length, the rigidity of the support material could influence metal binding [47]. The dense packing of the column could decrease their mobility, leading to a loss of binding sites when immobilized on the rigid supports. Consequently, the ion release is slower.

4. Applications of PASP in terms of chelation abilities

4.1. PASP as an industrial antiscalant

Undesirable mineral precipitation/deposition, referred to as scaling, can cause severe problems in various industrial equipment. The precipitated mineral gradually grows in size and accumulates, thereby

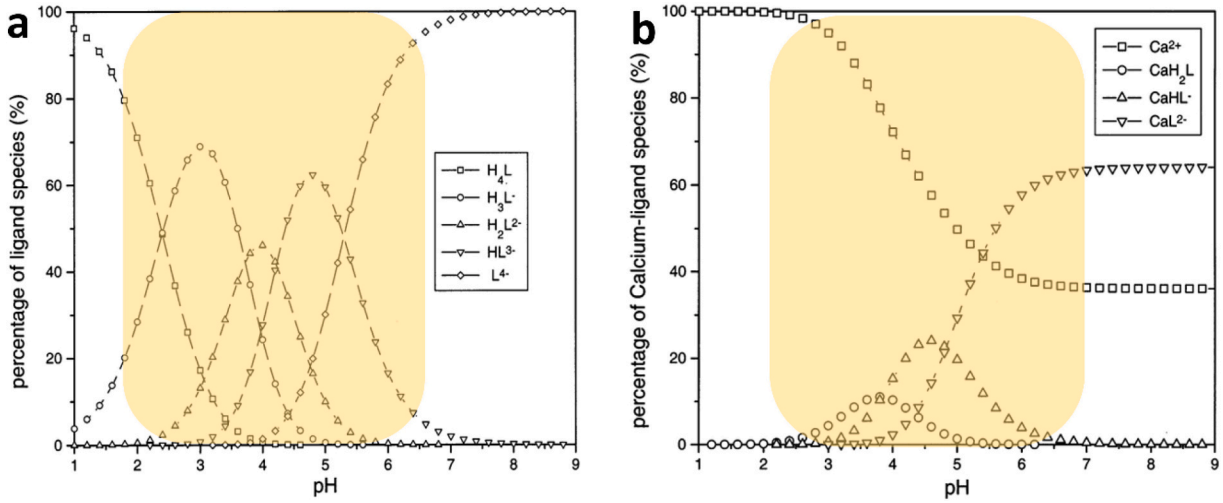

Fig. 3. Effect of pH on PASP ionization and chelation. (a) Different species of PASP (in percentage) as a function of pH. L is assumed as a hypothetical molecule consisting of four aspartyl monomers. (b) PASP-Ca complexation species (in percentage) as function of pH. In (a) the highlighted rectangle shows the pH range where different species of aspartyl ligands are formed, while in (b) the highlighted rectangle shows the area where calcium chelation is affected [39].

Table 2
The level of affinity of different ions with PASP is different. The pH and flow rate were 7, and 1 mL/min, respectively [37].

Metal ion	Capabilities (μmol/g) determined from breakthrough curves	Capabilities (μmol/g)[a] determined from acid strip	Recovery (%)
Fe^{3+}	36 ± 1	20 ± 4	54
Al^{3+}	26 ± 1	12 ± 10	46
Cu^{2+}	12 ± 1	12 ± 1	100
La^{3+}	7.1 ± 0.3	6.3 ± 0.4	89
Pb^{2+}	4.6 ± 0.1	4.5 ± 0.1	98
Cd^{2+}	3.7 ± 0.5	3.1 ± 0.1	84
Ni^{2+}	3.1 ± 0.2	2.9 ± 0.1	94
Co^{2+}	1.6 ± 0.1	1.6 ± 0.1	100
Mn^{2+}	1.5 ± 0.2	1.4 ± 0.1	93
Ca^{2+}	1 ± 0.1	1.2 ± 0.1	120[a]
Na^{+}	<0.1	<0.1	–

[a] The authors reported >100 % recovery that is not acceptable, but it was not explained by the authors.

obstructing the water flow and lowering the equipment efficiency (Fig. 4). The so-called target ion responsible for industrial scaling is predominantly calcium, while the counterion usually is sulfate, carbonate, and phosphate. Industrial antiscalants with extremely low levels (e.g., <20 ppm) are widely utilized to chelate the responsible ions thereby preventing their precipitation/deposition (Fig. 4d).

The need for green, sustainable, non-toxic, and biodegradable antiscalants such as PASP has been recently highlighted, given the importance of environmental protection [39,48–50]. PASP is regarded as a suitable substitute for non-degradable chelating agents such as ethylenediaminetetraacetic acid (EDTA), polyacrylic acid, and phosphorus-based inhibitors [51–53]. Below, the effect of PASP on calcium carbonate, calcium phosphate, and calcium sulfate as two important minerals is reviewed.

4.2. Effect of PASP on crystallization inhibition of calcium carbonate

Calcium carbonate ($CaCO_3$) is one of the main components of scaling in various industries. Its equilibrium reaction is as $Ca^{2+} + 2HCO_3^- \leftrightarrow CaCO_3 + H_2O + CO_2$ [54]. $CaCO_3$ occurs in three crystallite forms including aragonite, vaterite, and calcite, with the latter being the most stable and the most water-insoluble form. Although vaterite and aragonite are thermodynamically unstable, they can transform into calcite under appropriate conditions [55].

The addition of very small quantities of PASP and poly(glutamic acid) (PGA) (0.2–0.3 ppm), into the precipitation system (containing 1 to 2.5 mM of Ca^{2+} and $CO3^{2-}$) completely inhibited the crystal growth of calcite. PASP exhibited higher inhibition efficiency as compared to PGA which was attributed to better conformational matching between PASP and calcium atoms at the calcite surface [49]. In another study, comparison of PASP with poly(maleic acid) in terms of inhibition of $CaCO_3$ scale formation further verified PASP's superiority [56]. The addition of magnesium ions along with PASP to the precipitation system showed a synergistic impact on inhibition of $CaCO_3$ crystallization [50]. The presence of such ions is regarded as an impurity, which disturbs $CaCO_3$ crystallization.

Eichinger et al. [57] also showed that a low level of PASP not only decreased the amount of scale by around 7 tons/year in two tunnel drainage systems in Austria, but also reduced the structural integrity and compactness of the $CaCO_3$ scale, making deposits much looser and softer, thus helping to facilitate the removal of scale from the tunnel walls (Fig. 5a, b). Aside from porosity in the formed scale, a change in crystal structure of $CaCO_3$ from calcite to aragonite and vaterite was also observed by the addition of PASP. Similar results were obtained by Zou et al. [58] who found that at low concentrations of PASP, inhibition of crystallization of vaterite is more effective than that of calcite, while at high concentrations, vaterite formation is favored over calcite (Fig. 5c). These results are further supported by other studies [59,60]. In another study, electro-crystallization of $CaCO_3$ was monitored by optical microscope images which showed a dense calcareous film (similar to those without inhibitor) when the concentration of PASP was 1 ppm. However, at 4 and 10 ppm, the formation of vaterite, and the complete inhibition of crystallization were observed.(Fig. 5d) [59].

Interestingly, some studies have shown that PASP could even contribute to the dissolution of calcite [33,39]. At acidic pH valuess and in the absence of PASP, dissolution was dominated by the reaction of protons with calcite [33]. However, at alkaline conditions (e.g., pH = 10), dissolution occurred via Ca^{2+}-PASP complexation. Therefore, dissolution in neutral conditions was proposed to be a combination of these two mechanisms. Furthermore, increasing the pH decreased the dissolution rate, suggesting that chelation alone is a slow process when compared to the reaction of calcite with protons.

4.3. Effect of PASP on crystallization of calcium phosphate

Calcium phosphate (CaP) mineralization which gives rise to hydroxyapatite (HAp) [i.e., $Ca_{10}(PO_4)_6(OH)_2$] is particularly of utmost

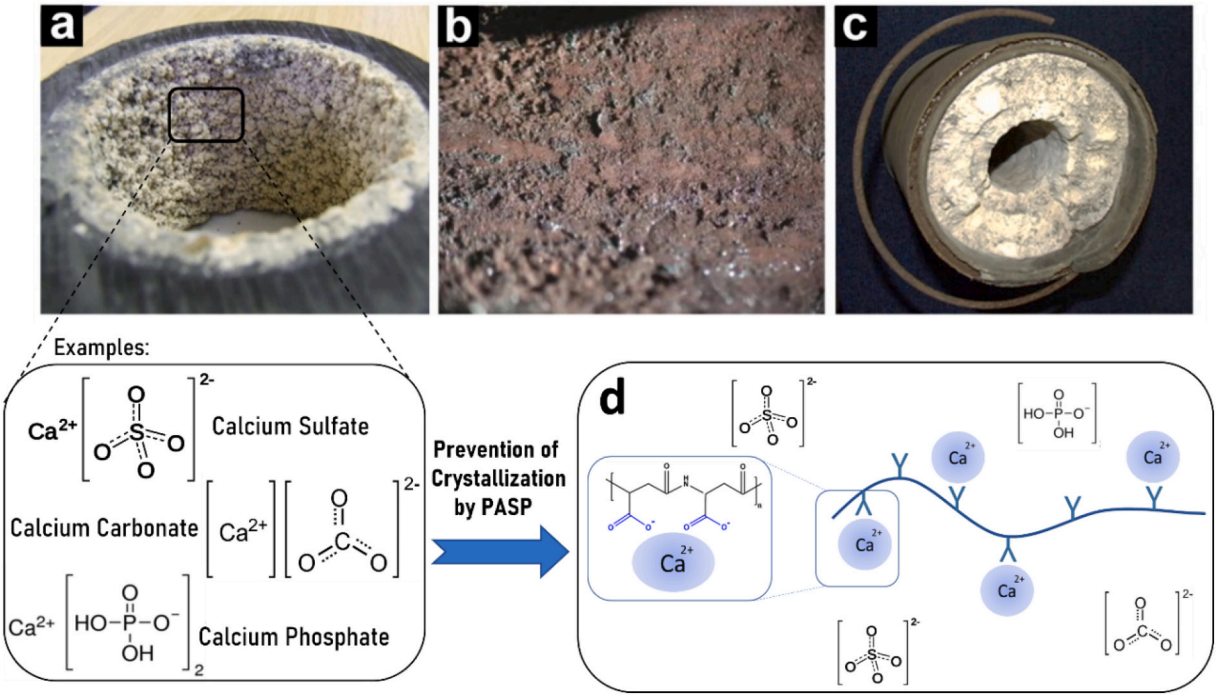

Fig. 4. Examples of scales and deposits: Deposit produced (a) in a pipe and (b) on the internal surface of economizer. (c) Struvite on the surface of pipe in a wastewater treatment plant [174]. The components of scale are shown to include but not limited to $CaCO_3$, $CaSO_4$, and CaP. (d) Precipitation, deposition and accumulation of such salts are inhibited in the presence of PASP which binds to calcium, deactivating it for interaction with the counterions (e.g., sulfate, carbonate, and phosphate), thereby leaving the counterions in the free form (i.e., soluble in water). Calcium chelation by PASP occurs through two adjacent ionized acidic groups of PASP, which bind to one calcium cation.

importance in as it is the main component of bone and dentin. Aspartic acid, among various amino acids, were found to have the highest affinity constant with HAp [61]. Nevertheless, a number of studies have shown that PASP as compared to aspartic acid monomer is much more effective in calcium chelation, suggesting the importance of polymeric nature of this amino acid in chelation, as also mentioned above [30–32].

Crystal inhibition, stabilization, and even dissolution of HAp have so far been reported using PASP [61–67]. Such a varied behavior can in part be explained by the contribution of several variables such as PASP to calcium ratio, phosphate concentration, and pH in the CaP mineralization and its corresponding equilibrium. For instance, Krogstad et al. [62] drew a boundary in terms of the concentration of PASP and Ca, above which the mixture of CaP precursor remained clear with time, suggesting complete inhibition of crystallization (Fig. 6-a). However, below the line where calcium level is high and PASP concentration is low, CaP aggregates formed.

At high concentrations of calcium (50–100 mM of Ca^{2+}), the presence of PASP, although ineffective in the complete inhibition of precipitation, led to a slower HAp crystallization and contributed to the oriented attachment of CaP particles, resulting in the formation of nanorods. Aggregates of CaP in the form of spherical particles were formed in the early stages of the reaction while nanorod-like crystals were formed at the end of crystallization (19–30 mg/mL of PASP). The aggregate to nanorod conversion was monitored by the change in optical density as the aggregates have higher turbidity as compared to nanorods, allowing one to follow the transition by a time-dependent decrease of optical density. The results demonstrated that the OD reduced as PASP concentration increased or calcium level decreases (Fig. 6b and c). The TEM images also demonstrated the morphology aggregate-to-nanorod transition. (Fig. 6 d, e, and f).

Regarding the dissolution of HAp, Poumier et al. [64] indicated that PASP and PGA can dissolve HAp if they are present in excess. The presence of free polypeptide in solution was necessary to overcome interfacial effects of adsorbed polymer on the HAp surface. Littlejohn et al. [65] also found Na-PASP efficient for removal of CaP in the form of HAp, and brushite (i.e., dicalcium phosphate dihydrate) from stainless steel surface especially under alkaline conditions. Surface cleaning activity of Na-PASP was comparable to sodium citrate but slower than EDTA. Such an activity can be viewed as equivalent to dissolution of the mineral. The optimum efficiency of PASP for the removal of brushite deposits was under pH 5 [66]. Overall, despite its importance in biology, the dissolution activity of PASP for CaP and the corresponding minerals is not studied well, and thus further investigation is required to provide conclusive results in this regard.

4.4. Effect of PASP on inhibition of calcium sulphate crystallization

The build-up of calcium sulphate compounds represents a challenge especially in offshore oilfield machinery such as water injection systems used to mobilize oil. The precipitation of sulphate salts is attributed to the large amount of SO_4^{2-} in seawater (8 % [68]) reacting, Ca^{2+}, Ba^{2+}, and Sr^{2+} that occur naturally at high concentrations within the rock pores. As depicted in Fig. 7a, seawater contains approximately 3.5 % of different salts of which 8 % is sulfate. Industrial calcium sulphate scaling occurs by forming $CaSO_4$ (anhydrite), $CaSO_4.H_2O$ (hemihydrate), and $CaSO_4.2H_2O$ (gypsum). Rabizadeh et al. [34] evaluated the effect of different anionic polymers including PASP on the crystallization of calcium sulphate [gypsum type: dihydrate ($CaSO_4.2H_2O$)] by assessing turbidity. It was shown that as low as 20 ppm of PASP (M_w 5–10 kDa) completely inhibited gypsum formation for high concentrations of calcium (100 mM) and sulphate (100 mM), whereas poly(epoxysuccinic acid) (PESA), and high-M_w PAA (~100 kDa) were found to be ineffective (Fig. 7b). In contrast to the high-M_w PAA, low-Mw PAA (~2 kDa) decreased the rate and the extent of crystallization, yet with lower efficacy compared to PASP, highlighting the importance of short chain length in chelation.

Various other studies have also shown the effectiveness of PASP on the inhibition of calcium sulphate scaling [60,69–72]. Silica

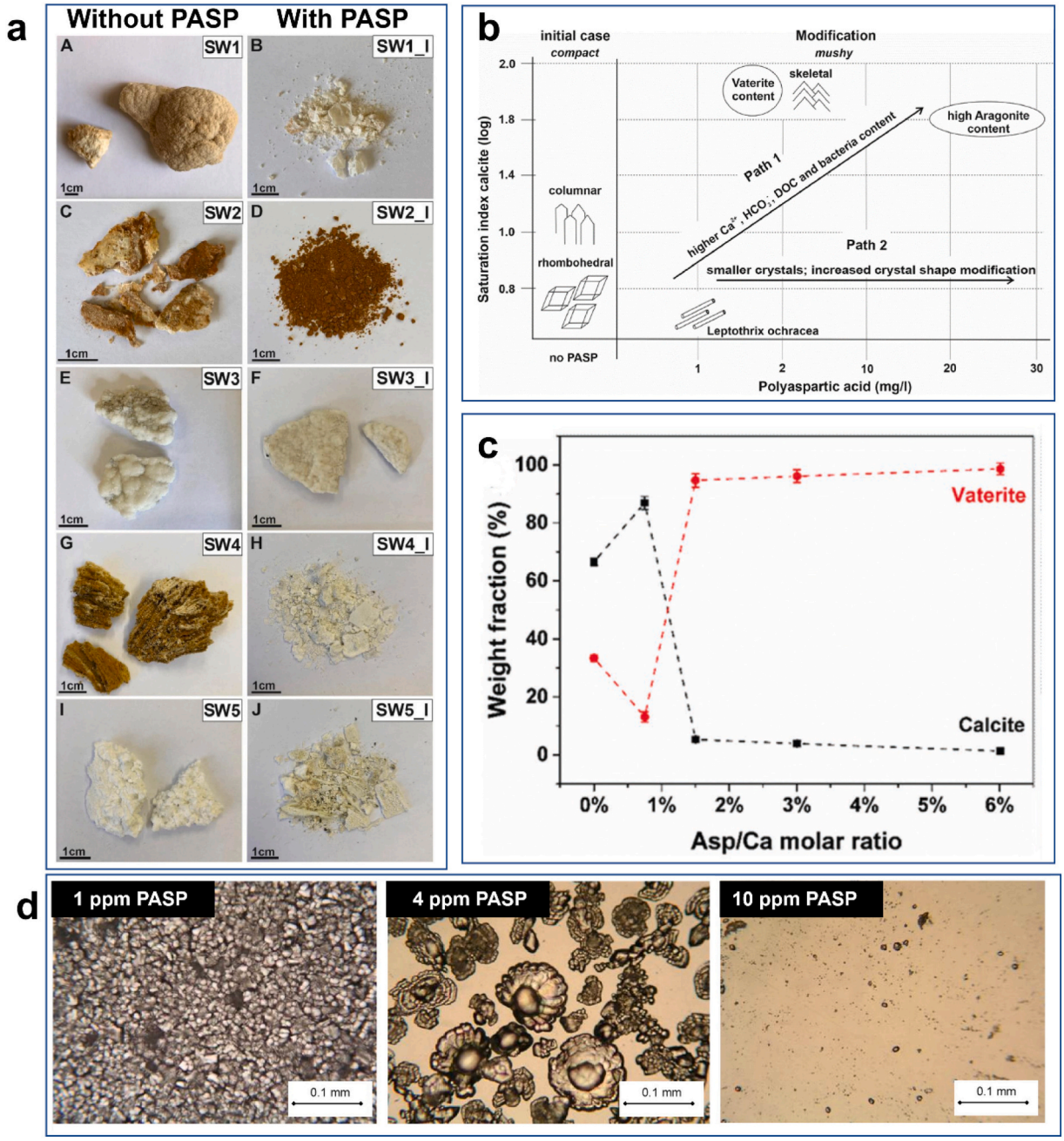

Fig. 5. The effect of PASP on crystallization, dissolution, and morphology of $CaCO_3$. (a) Macroscopic photographs of $CaCO_3$ scale in the presence and absence of PASP shows that the polymer makes the scale loose and weak in terms of mechanical properties. The samples were taken from different tunnel drainage systems in Austria viz. tunnel Spital (SW1–2) and tunnel Steinhaus (SW3–5) [57]. (b) Schematic illustration of different regions of $CaCO_3$ crystallization as a function of PASP concentration. The introduction of the polymer led to prevention of calcite formation (columnar and rhombohedral shape) while at high calcium level, aragonite and vaterite were formed. [57]. (c) The weight fraction of calcite and vaterite formed by electrodeposition of $CaCO_3$ as a function of ASP/Ca molar ratio, showing that at low and high concentrations of PASP, calcite and vaterite formation are dominant, respectively [58] (d) Optical microscopic images of $CaCO_3$ deposition through electro-crystallization with 1, 4 and 10 ppm of PASP after 24 h, showing a dense calcareous film, vaterite crystals, and complete inhibition of crystallization, respectively [59].

nanoparticles (NPs), due to small size and consequently large surface area, were used as a template for conjugation of PASP [73]. The precursor of PASP, i.e., PSI, reacted with amine groups of the NPs (Fig. 7c). The remnant succinimide units were converted to aspartic acid by alkali hydrolysis, and subsequently, the PASP-modified NPs were used as antiscalants for the prevention of calcium phosphate salt formation. Such an approach could be highly efficacious in the prevention of scale formation, and also in the elimination of (hazardous) ions from water because the NPs could easily settle/sediment due to reduced colloidal stability as a result of charge screening induced by chelation as well as high ionic strength.

The PASP-modified silica NPs had higher efficiency when compared with PASP, which was attributed to a higher COOH content in the former (Fig. 7d). However, the authors did not mention where the higher levels of COOH groups originates from. Of note is that temperature has a considerable impact on the solubility limit of most salts of calcium such as $CaCO_3$, and $CaSO_4$ where an increase in temperature is associated with a reduced solubility limit, thereby intensifying precipitation and

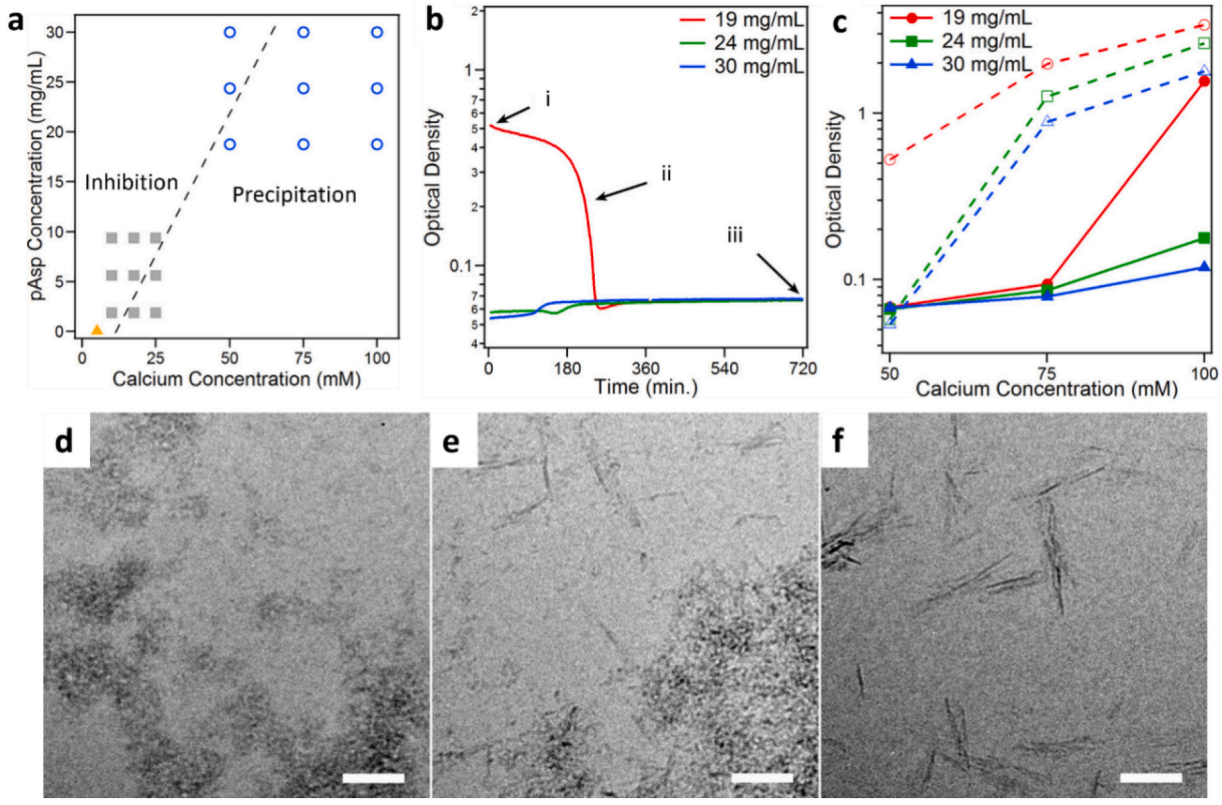

Fig. 6. The effect of PASP on crystallization, dissolution, and morphology of CaP. (a) Precipitation/crystal inhibition regimes as a function of PASP and Ca concentration. Above the line, the solution is clear, suggesting a complete inhibition of mineralization while below the line the solution is cloudy, reflecting the CaP precipitation [62]. (b, and c). Plots of optical density (OD) at 650 nm: (b) OD recorded every 60s for 24 h. Calcium concentration was 50 mM Ca^{2+} while the polymer concentration was varied. (c) The OD value at the start and the end of experiment respectively shown by open and closed symbols; different calcium concentrations (50, 75, and 100 mM) and polymer concentration (19, 24, and 30 mg/mL). (d, e, and f) The TEM micrographs of CaP aggregates at 19 mg/mL of polymer and 0.05 M of Ca^{2+} at (d) 15 min, (e) 4 h, and (f) 24 h, indicating the formation of large aggregates in the beginning followed by their dissociation and conversion to nanorods.

crystallization [13]. Therefore, particularly in industrial equipment where hot water is in circulation (e.g., heat exchangers), scale formation of such minerals is more conspicuous and thus creates enormous challenges. As seen in Fig. 7e, increasing the temperature from 70 °C to 90 °C reduced the inhibition efficiency from 100 % to around 20 % for PASP and to approximately 40 % for PASP-modified silica. This shows that the decreased solubility of calcium sulfate salt at elevated temperatures was severe enough to significantly reduce the inhibitory role of the polymer [73]. The role of calcium and polymer concentrations were also investigated [74]. Obviously, the lower the amount of polymer, the higher the level of calcium salt formation. Similarly, the higher the level of calcium, the higher calcium salt formation (Fig. 7f, g).

While components of scale mostly include the minerals discussed above, it is not limited to them. Depending on the industry and the process, various other minerals such as barium sulphate ($BaSO_4$) [52] and strontium sulphate ($SrSO_4$) [53] could be involved in the formation of scale where PASP was found to be highly efficacious in these cases too [52,53]. In conclusion, PASP as an antiscalant lowers the activity of ions through complexation and/or by adsorption onto the surface of preformed salts, preventing further growth of the scale [33,34]. If the ion concentration is far above supersaturation, PASP may still function by reducing crystallization rate, changing the crystal morphology, and functioning as a stabilizer to prevent increases in the size of precipitated particles. Overall, the concentration of PASP commonly employed in studies (<20 ppm) is much lower than the stoichiometric equivalent of ions in the system, suggesting that scale inhibition is not just sequestration of salt-forming ions and that the antiscalant can block active and growth sites of insoluble salts [13].

4.5. Stabilization of inorganic (nano)particles by PASP

Due to both chelation ability and negative charge, PASP could potentially function as a stabilizer for a variety of inorganic (nano) particles (NPs) where a metal, transition metal, or an alkaline earth metal is a major constituent. Chelation ensures robust attachment of PASP onto NP surface, while the negative charges provide electrostatic stabilization, repelling the adjacent NP by the negative charge, thereby preventing aggregation (Fig. 8a). Polymeric nature of PASP, which provides steric hinderance, could be considered as another reason for the good colloidal stability [75].

The use of PASP significantly enhanced dispersibility of barium titanate, which is a widely used dielectric agent in multilayer ceramic capacitors [76]. The introduction of PASP at pH 5 was accompanied with a charge reversal in the particles. The increase in zeta potential values to more negative values suggested successful attachment of PASP on the particle surface (Fig. 8b). The higher sedimentation density (i.e., lower sedimentation volume) in the presence of PASP confirmed the enhancement of the colloidal stability (Fig. 8c) [76].

Pure PASP was also shown to improve dispersibility of manganese oxide NPs in water [77]. The NPs were prepared in hexane where they had a good level of colloidal stability, whereas no dispersion could be achieved in water. The addition of PASP completely transferred the NPs from the oil phase to water phase (Fig. 8d, e). Comparison of PEG with PASP showed that the latter provides much better stability after 4 months of storage (Fig. 8f). Pure PASP has also been used as a reducer and as a stabilizer for in-situ synthesis of gold NPs (size of around 55 nm) [78].

Jana et al. [15] grafted cysteine to PASP and demonstrated that the

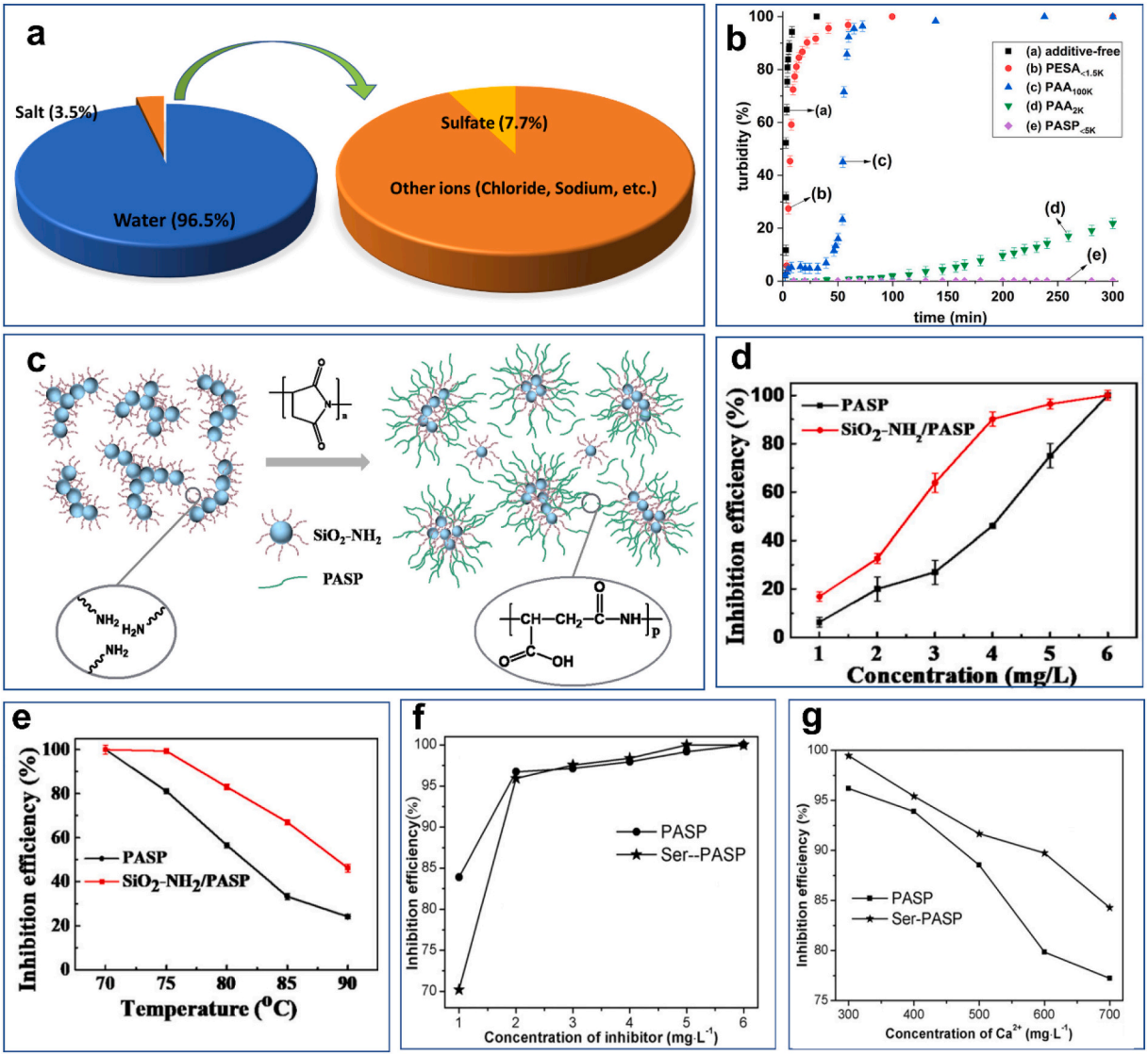

Fig. 7. The effect of PASP on calcium sulfate. (a) Amount of salt in seawater (approximately 3.5 %), of which around 8 % is sulfate. (b) Inhibition of gypsum crystallization by the addition of different types of antiscalants including PASP (20 ppm, pH = 7) [34]. The turbidity level corresponds to the extent of salt formation and gypsum crystallization. (c) Schematic representation of surface modification of silica NPs with PSI followed by alkali hydrolysis, resulting in PASP-modified silica NPs [73]. (d) $CaSO_4$ inhibition efficiency of PASP and PASP-modified silica NPs, showing the superiority of the latter [73]. (e) The effect of temperature on the inhibition efficiency: inhibition efficiency is reduced by increasing temperature both for free PASP and immobilized PASP on the surface, which is due to reduced solubility of calcium salts at elevated temperatures rather than reducing polymer activity [73]. (f, and g) Inhibition efficiency as a function of inhibitor concentration (f) and calcium concentration (g) for PASP and serine-grafted PASP: increasing the polymer concentration and reducing calcium level both improve inhibition efficiency [74].

thiolated polymer is highly effective in improving the colloidal stability of a variety of hydrophobic nanocrystals such as silver NPs, gold NPs, and CdSe@ZnS quantum dots (Fig. 8g). Apart from the chelation ability of PASP, the presence of thiol groups ensured robust attachment of the polymer onto the surface of the nanocrystals, while the carboxylic acids improved the colloidal stability, and provided the NPs with the ability of further functionalization with antibodies and other reagents. The nanocrystals covered with the polymer exhibited higher biocompatibility [15]. Interestingly, PSI which is the anhydrous form of PASP was successfully applied for in-situ synthesis of silver NPs in DMF solvent. Stable particles were achieved which could potentially originate from the interaction of silver ions with functional groups (i.e., aspartic acid) at the end of PSI chains [79].

Despite these advantages, pure PASP may not be able to provide sufficient stability in certain cases which require one to modify the chemical structure. Grafting of long alkyl chains to PASP has shown to provide surface-active (i.e., surfactant) properties for stabilization of hydrophobic NPs [80]. For instance, dodecyl (i.e., C12) grafted-PASP significantly enhanced dispersion of manganese (IV) oxide NPs in water [81].

A number of studies have also shown that both pure PASP and modified PASP could improve the dispersion ability of ferric oxide in water which is of utmost importance not only in corrosion inhibition but also in magnetic resonance imaging (discussed below in biomedical applications of PASP) [74,82,83]. Overall, as a conclusion, one can correlate the chelation ability of PASP to the improved stability of inorganic colloidal systems. Accordingly, and in light of the studies reviewed above, PASP could find more use as a stabilizer of slurries and particles in the future.

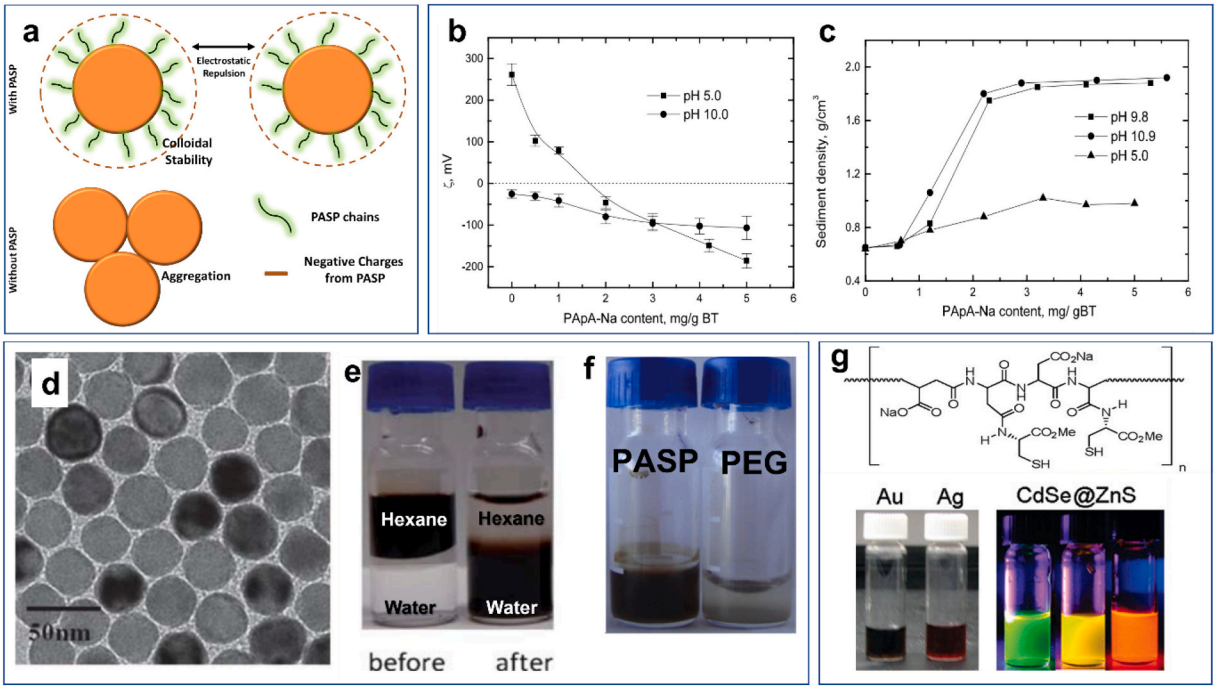

Fig. 8. PASP for improving colloidal stability. (a) Schematic representation of colloidal stability because of the PASP coating. The PASP chains on the surface of NPs improve colloidal stability through electrostatic repulsion. (b) Zeta potential and (c) sedimentation density of barium titanate (BT) particles vs. PASP concentration. Under different pH conditions. PApA-Na refers to sodium salt of PASP. The higher the sedimentation density (equal to lower sedimentation volume), the better the colloidal stability [76]. (d) TEM micrographs of MnO NPs with the average diameter of 35 nm. (e) PASP effectively attached on the surface of hydrophobic MnO NPs and transferred them from hexane as the oil phase to water phase [77]. (f) PASP-treated MnO NPs were stable after 4-months storage, while PEG-treated NPs showed complete sedimentation [77]. (g) Molecular structure of the cysteine-grafted PASP. The thiol (SH) groups attach strongly onto the surface of the nanocrystals while carboxylic acid groups provide electrostatic repulsion for colloidal stability. The photograph shows colloidally stable gold NPs, silver NPs and CdSe@ZnS quantum dots [15]. (For interpretation of the references to color in this figure legend, the reader is referred to the web version of this article.)

4.6. PASP as an additive for wine preservation

Potassium bitartrate is formed in wine containers during fermentation of grape juice. Because of the supersaturation of potassium and tartaric acid, as well as low water solubility of the salt, potassium bitartrate is crystallized during fermentation, precipitated, and deposited in wine bottles and containers. PASP can prevent such precipitation by inactivating potassium through chelation. Thanks to its biocompatibility, PASP could be regarded as an edible additive prior to wine bottling without the need for further purification/separation. Recently, potassium salts of PASP were approved as additivea for tartaric stabilization in wines (OIV/OENO 543–2016) and is being used by many European wineries [16,84]. In comparison to metatartaric acid (MTA) and carboxymethylcellulose (CMC), as other commonly used inhibitors, PASP neither adversely affects the wine color, nor leads to haze formation over time [16]. PASP with different M_w values (3, 5, 10, and 15 kDa) were all found effective in the prevention of tartaric precipitation after 1 year of bottle aging [85]. PASP had similar effectiveness as MTA especially in red wines [86]. However, in the long-term, PASP showed much more stability than MTA. After 1 year of wine aging, PASP maintained its stabilizing effect regardless of M_w, whereas MTA entirely lost its effectivity. The release of monomeric aspartic acid from PASP because of polymer degradation was also studied after 5- and 12-months storage. 1.9 % and 6.3 % of aspartic acid with respect to the initial weight of PASP was released in the white and red wine, respectively. It was found that PASPs with the lowest monomer release provided better wine stability [86]. Recently, the effects of PASP (potassium salt), CMC, and MTA were compared on variety of wines (including Chardonnay and Rhein Riesling), further confirming the superiority of PASP. Interestingly, PASP could stabilize the wines even at half the recommended dose after 175 days storage [87].

4.7. Corrosion inhibitor

Corrosion is a vital challenge in variety of industrial processes ranging from chemical production to power generation. It can cause catastrophic accidents and economic loss and thus should be mitigated and minimized by using efficient corrosion inhibitors [88–90]. Compared to small molecule compounds, long-chain polymers, such as PASP, generally exhibit higher inhibition performance [91,92]. By the formation of a protective layer at anodic/cathodic sites on the metal surface, PASP can serve as an efficient inhibitor, retarding metal dissolution. In other words, PASP not only limits water access to the metal surface but also restricts oxygen diffusion, thereby acting as a barrier against metal dissolution in the electrolyte and could reduce the anodic reaction of corrosion [88].

The corrosion inhibition ability of PASP could stem from the formation of stable PASP-metal ion complexes on the metal ions. PASP concentration has a direct relationship with the inhibition efficiency which could probably be attributed to the formation a denser layer on the metal surface. For example, with increasing PASP concentration from 0.1 to 4 g/L for carbon steel in 0.5 M sulfuric acid, the inhibition efficiency improved from 39 % to 80 % [93]. For WE43 magnesium alloy in a 3.5 wt% NaCl solution, maximum efficiency of 94 % was obtained with 400 mg/L of PASP [94].

The corrosion inhibition performance of PASP could be further improved through chemical modification of the polymer [92] or combination with other anti-corrosion agents such as zinc [95]. For instance, cysteamine-grafted PASP, contains sulfhydryl groups, and this modified polymer exhibited a better corrosion inhibition performance than pure PASP for mild steel in a medium containing a high concentration of sulfuric acid (0.5 M) [91]. Likewise, dopamine-grafted PASP showed a good corrosion performance in acidic solutions for mild steel [96]. This was correlated to efficient adsorption of the modified polymer on the

metal surface through donor-acceptor interactions between unfilled *d*-orbitals of Fe and π-electrons of dopamine. Of note is that dopamine itself has a high affinity with iron ions and iron-dopamine complexes have been used for polymer crosslinking [97,98]. Modification of PASP with a Schiff base structure on carbon steel in a HCl solution (1 M) was also evaluated [92]. The grafted Schiff base structure with imine groups on PASP created a superior anti-corrosion effect where only 80 ppm of the inhibitor provided a maximum inhibition efficiency of about 90 %. Such a high efficiency was attributed to synergistic effect of both PASP and the Schiff base. The latter was found to be effective as an anti-corrosive agent due to imine group (–CH=N–) [99,100].

Due to simplicity in polymer modification through ring opening of succinimide groups in the precursor polymer, which will be discussed below, a variety of other active reagents have been employed for enhancement of the inhibition efficiency. For instance, *β*-cyclodextrin-grafted PASP provided a strong corrosion inhibition activity for N80 carbon steel in a solution containing $MgCl_2.6H_2O$, NaCl, $CaCl_2$, Na_2SO_4, and $NaHCO_3$. With 800 mg/L of the polymer, a corrosion rate of 2.94×10^{12} m/s, and inhibition efficiency of 68 % were obtained [89]. Glycine-grafted PASP at a concentration of 250 mg/L was also introduced as an effective inhibitor for X-65 carbon steel in seawater with an inhibition efficiency of about 84 % [90]. It is worth mentioning that the addition of other anti-corrosion agents such as 2-hydroxyphosphonoacetic acid, and zinc sulfate to PASP could lead to a synergistic effect [88,101]. Excellent anti-corrosion of carbon steel was demonstrated by the use of the mixture (Fig. 9 a, b) [101]. Analysis of the polarization curves showed a decrement in the corrosion current by the introduction of the mixture (Fig. 9b). The corrosion potential also shifted to more anodic values, suggesting that anodic type inhibition. It was postulated that the polymer chelates to iron ions on the steel surface. The presence of zinc ions was also reported to encourage the precipitation of polymer on the surface, further enhancing the formation of protective film [101].

By self-assembly, Wang et al. [102] prepared PASP-zinc films on Q235 steel surface. Pure PASP films were assembled as monolayers with a loose and thin structure, whereas PASP-zinc films exhibited a rough morphology with a large number of NP and a thickness of approx. 100 nm. The presence of zinc along with PASP was found to be necessary for achieving a high corrosion inhibition efficiency (Fig. 9c, d). The polarization curves showed that the corrosion potential shifts to more negative values by the addition of PASP, suggesting that the corrosion inhibition stem from inhibition of cathodic reactions through adsorption (Fig. 9c). It was proposed that the PASP-zinc layer that formed on the surface isolated the corrosive medium from metal through bonding to the metal surface (Fig. 9d). Another study also confirmed the synergistic role of zinc together with PASP by investigating the corrosion mechanism [95]. It was shown that zinc improves the film thickness due to excellent coordination ability, thereby preventing the steel surface to be exposed to corrosive agents. Nevertheless, in contrast to Wang et al. [102], it was suggested that iron on the surface is replaced with zinc-PASP complex [95].

4.8. PASP as chelator in water remediation

The importance of PASP in prevention of scale formation was stated above. Accordingly, PASP has successfully been employed in reverse osmosis membranes as an anti-scaling agent for water purification [103]. However, aside from calcium, PASP has a high affinity with other metal ions. Contamination of water and soil with a variety of contaminants including heavy metals is now a serious environmental concern all over the world. In this regard, the use of chelating agents as a remediation technology can form strong water-soluble complexes with toxic metals to reduce toxicity and activity of the ions [104]. In comparison with conventional chelators like EDTA, PASP is regarded as being much safer in terms of both biocompatibility and biodegradability and thus has great promises in remediation field [105,106]. Compared to small molecules, PASP, as a polymeric chelator, can be designed in different physical forms including but not limited to fibers, particles, beads, films, and foams for effective removal and elimination of the ions. In addition, to ensure prevention of PASP dissolution, its immobilization [43] or crosslinking [107] is also required. For crosslinking PASP-based

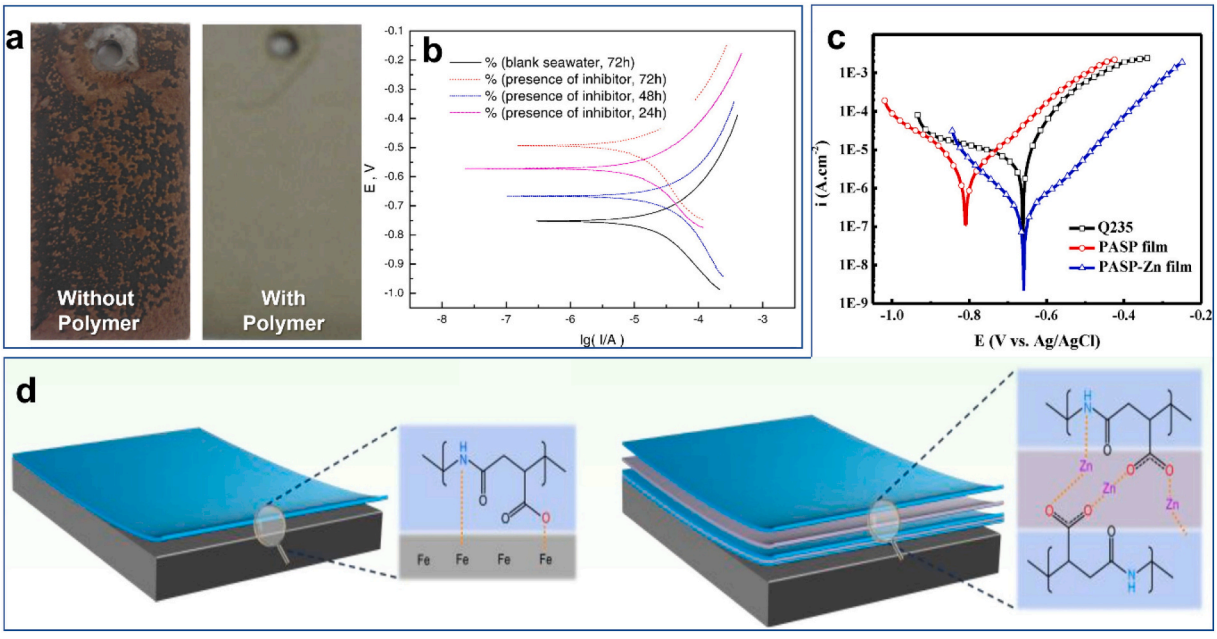

Fig. 9. Corrosion inhibition of PASP (a) Photographs from the surface of carbon steel exposed to seawater without and with 0.1 g/L of PASP-SEA-ASP (SEA: 2-aminoethanesulfonic acid; ASP: aspartic acid) [101]. (b) Polarization curve of the steel at different time points with and without corrosion inhibitor. E, V is potential in volts, while Ig (I/A) is electric current density in ampere per square centimeter, where the reference electrode was a standard calomel electrode (SCE) [101]. (c) Polarization curves of bare Q235 steel, coated with PASP and Zn-PASP. i ($A.cm^{-2}$) is the current density while E (V vs. Ag/AgCl) is the potential in volts versus Ag/AgCl as reference electrode [102]. (d) The proposed mechanism for corrosion inhibition is the chelation of iron ions on the steel surface by PASP, and the formation of a second polymer later through mediation of zinc [102].

hydrogels have been prepared [8], which contributed to efficient ion removal, as the complexed ions can be eliminated from water by removing the gel. Hydrogels based on PASP have also shown promising results for water purification. For instance, glutaraldehyde cross-linked hydrogels of chitosan/PASP chelating resin with carboxylate anion, amino, and amide groups played a significant role in Hg^{2+} (q_m = 170 mg/g) and Pb^{2+} (q_m = 152 mg/g) adsorption [108]. In another study, a commercial form of PASP was used to remove Zn^{2+}, Cu^{2+}, Pb^{2+}, and Cd^{2+} from wastewater [17]. The polymer-ion complexes were then absorbed via electrostatic attraction on chitosan. Dopamine-conjugated PASP biodegradable hydrogels were shown to adsorb large quantities of metal ions from aqueous solutions [109]. By increasing the metal ion valence ($Na^{+} < Ca^{2+} < Fe^{3+}$), the hydrogel swelling decreased, which could be due to the different ion bonding abilities of catechol and carboxylate groups. The former has a good affinity towards iron ions rather than sodium and calcium. Furthermore, reduced swelling is attributed to charge screening due to the introduction of counterions. Composite hydrogels made of PASP/carboxymethyl poplar sawdust also demonstrated high level of Cd^{2+} removal [110]. Recovery of Cd^{2+} and Cu^{2+} from the water was accomplished by applying a chelating PASP resin [111]. PASP structure had a good selectivity for Cu^{2+} in a binary system containing Cd^{2+} and Cu^{2+}. This sorbent was regenerated by acid solution (HNO_3), which indicated an efficiency of about 90 % for at least five regeneration cycles.

Rapid and simple detection of metal ions both in water and soil is of great importance. An electrochemical sensor based on PASP grafted on gold electrode was developed. The aspartic acid chain length was in the range of 32–96 aspartic acid units. Due to the high affinity of PASP towards Cu^{2+}, extremely low detection limit of 3 nM (0.2 ppb) was obtained with voltammetry method [112]. Inexpensive colorimetric sensors were developed for the detection of Fe^{3+} and Cu^{2+} by PASP nanofibers [113]. Electrospinning method was employed for the preparation of the nanofibers (Fig. 10a). The sensors showed detection limits of 0.3 mg/L and 0.1 mg/L for Cu^{2+}, and for Fe^{3+}, respectively. Upon

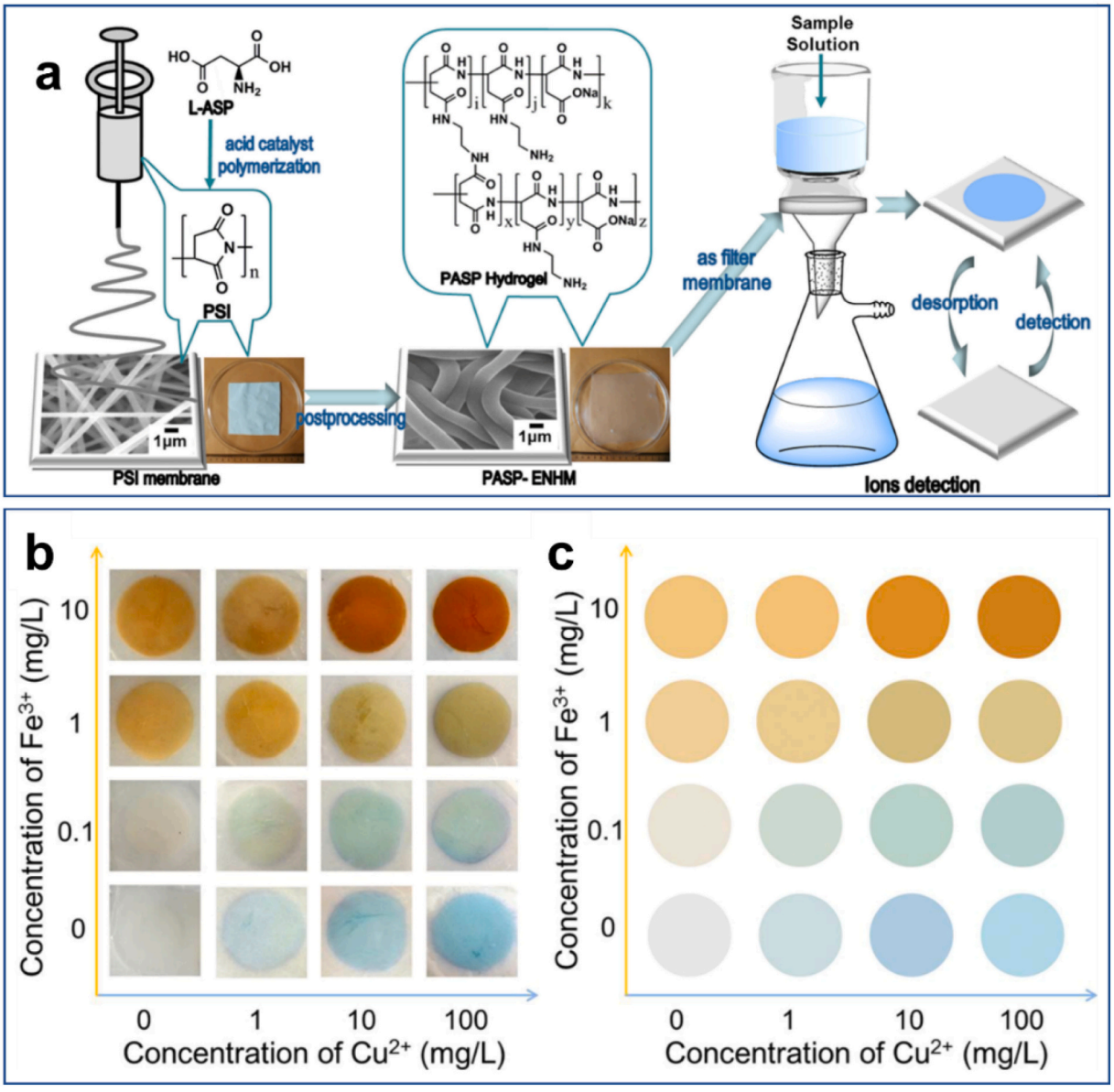

Fig. 10. PASP-based sensors for detection of iron and copper. (a) Development of crosslinked PASP nanofibers by electrospinning for detection of copper and iron ions (b) Macroscopic photographs of the nanofiber hydrogels after being exposed to water containing different iron and cupper ions. (c) The reference color map established according to the color changes on the sensors in shown (b), by which one could realize the iron, and copper concentration of water simply by the naked eye [113].

increasing the former and the latter ions, the sensor's color changed from white to blue, and white to yellow, respectively (Fig. 10b). Based on the color changes on the sensors, a reference color map was established through which one could realize the iron, and copper concentration of water simply by the naked eye (Fig. 10c). Desorption of the complexed ions by a strong acid could recover the sensors [113]. Despite being highly efficient in the detection of these copper and iron, the interference of other ions such as calcium, magnesium, etc. was not investigated. In another study, PASP was used in the perfusion liquid to enhance microdialysis. Different metal ions such as Cr, Ni, Cu, and Pb were tested in which PASP was found highly efficient with high relative recovery values. PASP was far better as compared to poly-l-histidine for all metal ions tested [114]. Further enhancement in the recovery was achieved when a combination of PASP, poly-l- histidine and 8-hydroxyquinoline was used in the perfusion liquid [115,116].

As a polyelectrolyte, PASP could also be applied in the electrokinetic remediation of pollutants in soil where a low direct current of up to 1 A or a low and direct electric-voltage gradient of up to 2 V/cm across the electrode transfer contaminants in soil towards the electrodes [42]. Acidification of soil could desorb toxic metals from the soil. Simultaneous use of both PASP and citric acid was shown to effectively reduce Cr^{6+} to Cr^{3+}, which masks the toxic effect of free ions [42].

4.9. Chelation ability of PASP in biomedical areas

Due to high biocompatibility and biodegradability, PASP meets the basic requirements to be used in biomedical applications as a metal-binding polymer. Biomedical applications of PASP were reviewed recently, which revealed that little focus has been paid to PASP's chelation ability [20]. Chelation therapy is defined as a type of medical treatment for lowering and/or eliminating the toxic impacts of metals ions, particularly that of heavy metals. The ion-chelator complexation can occur in either intracellular or extracellular spaces, forming less toxic species with lower activity. The chelated ions are subsequently excreted from the body with either no or minimal adverse effects.

PASP modified with L-cysteine was used to treat lead poisoning in mice via oral and intraperitoneal administrations [117]. The polymer efficiently removed lead accumulated in different organs, while it did not affect the essential metal ions such as copper, iron, zinc, and calcium. Such a high selectivity towards Pb^{2+} is attributed to the presence of cysteine groups in the polymer structure. However, even without any modification, PASP was found to be remarkably efficacious in reducing the toxicity induced by Pb^{2+}, Cu^{2+}, and Cd^{2+} on zebrafish (*Danio rerio*) [105]. After 24 h exposure, the LC_{50} of these ions were found to be 5.15, 2.82, and 0.09 mg/L, respectively. No death was observed in the PASP-treated groups, revealing the chelation ability of the polymer through which toxicity was alleviated [105]. PASP-based polymers has also reduced toxicity of iron-oxide NPs as reported in different studies, which could be related to its iron chelation [118].

Polymer gels that respond to external stimuli, are well known as promising new class of materials [119]. PASP as an anionic biocompatible polymer responds to changes in ion concentration and pH. Ionic strength can strongly shield the negative charges along the chain of PASP that originates from carboxylates, thereby collapsing the chain conformation. Metal ion complexation of PASP further strengthens this property, meaning that in the presence of calcium, for example, the gels could undergo a remarkable water loss, and reduced swelling when it is compared to deionized water. [119].

Aside from pH and ionic strength, PASP can be modified to respond to other stimuli as well. For instance, thiolated-PASP nanogels were shown to effectively respond to the redox state of the medium and thus could be employed for drug delivery/release systems [120,121]. The cleavage of disulfide bonds by a reducing agent led to the degradation/disintegration of nanogels, resulting in the release of the encapsulated drug. Due to the similarity of the PASP structure with the extracellular matrix, and the fact that its backbone is similar to that of protein, it could be applied as a promising scaffold for cell proliferation [7]. The presence of thiol groups in such structures could even further facilitate cell adhesion and proliferation [122]. Therefore, thiolated PASP gels could particularly serve as suitable ones for osteosarcoma cell cultivation. Moreover, modification of PASP hydrogels with biological molecules like dopamine could also improve adhesion, migration, and proliferation [123]. It is noteworthy to mention that calcium ions regulate the adhesion, proliferation, and overall function of a variety of cell types through calcium signaling and calcium channels [124]. Hence, the high level of cell proliferation of PASP-based scaffolds mentioned in the studies above could be attributed to calcium chelation of PASP, although this hypothesis has not been studied and proved yet.

Through iron and copper chelation, PASP can regulate the level of reactive oxygen species (ROS). Although low concentrations of ROS are essential in maintaining proliferative signaling, growth and cell survival, chronically high concentrations are detrimental, due to DNA damage [125]. ROS (e.g., hydroxyl radicals) are produced from the Fenton reaction using transition metals such as Fe^{2+} or Cu^{+} as catalysts (Eqs. (1) and (2)). Therefore, deactivation of these transitional metals could lead to anti-inflammation and potentially an anti-ROS approach [126].

$$Fe^{2+} + H_2O_2 \rightarrow Fe^{3+} + \dot{O}H + OH^- \quad (1)$$

$$Cu^{+} + H_2O_2 \rightarrow Cu^{2+} + \dot{O}H + OH^- \quad (2)$$

Furthermore, in analogy to industrial antiscalants which was discussed above, PASP can be efficacious in chelation therapy to prevent undesirable salt precipitation insoft tissues. A brief discussion is made below in this regard on the potential use of PASP for treatment of kidney stones and vascular calcification. Calcium-binding ability of PASP has also been used for targeting of drug-loaded nano-carriers to bone which is also discussed below.

4.9.1. Kidney stone and PASP

Kidney stones impact a large fraction of the world's population. Nearly 80 % of kidney stones are partially or completely made up of calcium oxalate monohydrate (COM). Calcium oxalate salts are generally highly water-insoluble with the formula CaC_2O_4 $(H_2O)x$, where x varies from 0 to 3 (Fig. 11a). As the stone size increases, ureter blockage occurs, causing pain and variety of complications. Human urine under normal conditions is usually supersaturated with calcium and oxalate ions. However, COM formation does not occur due to the presence of urinary inhibitors such as uropontin (uOPN) [127–130]. The latter is the human urine-isolated OPN and is a potent inhibitor of COM formation thanks to ASP residues as mentioned above [131,132].

Inhibition of COM crystal growth by PASP could suggest that close proximity of a series of ASP units in the OPN structure might also contribute to the prevention of crystal growth [133–135]. Accordingly, several studies have shown the effectiveness of PASP for inhibition and even dissolution of COM [31,32,136,137]. However, ASP monomer has no or little effect on the crystal inhibition of COM, again verifying the importance of its polymeric nature as discussed above [31,32]. The effectiveness of PASP was 16 times higher than that of PGA [32]. Polycations (i.e., cationic polyelectrolytes) such as poly-arginine and polylysine had negligible effects on the inhibition of crystallization which could be attributed to electrostatic charge repulsion, between positively charged COM and polycations [136]. Other studies have also indicated the superiority of PASP as an edible polymer to prevent COM buildup [138]. Comparison of PASP (M_w of 11 kDa) with uOPN revealed higher efficacy of the PASP in terms of inhibition of crystal growth. However, uOPN was found to be stronger for the prevention of COM crystal aggregation (Fig. 11b) [133]. Aggregation of COM is an important step in enlargement of the stone, and blockage of urinary tract. Therefore, stabilization of COM against aggregation could contribute to painless and easy excretion of COM from the body [131,139].

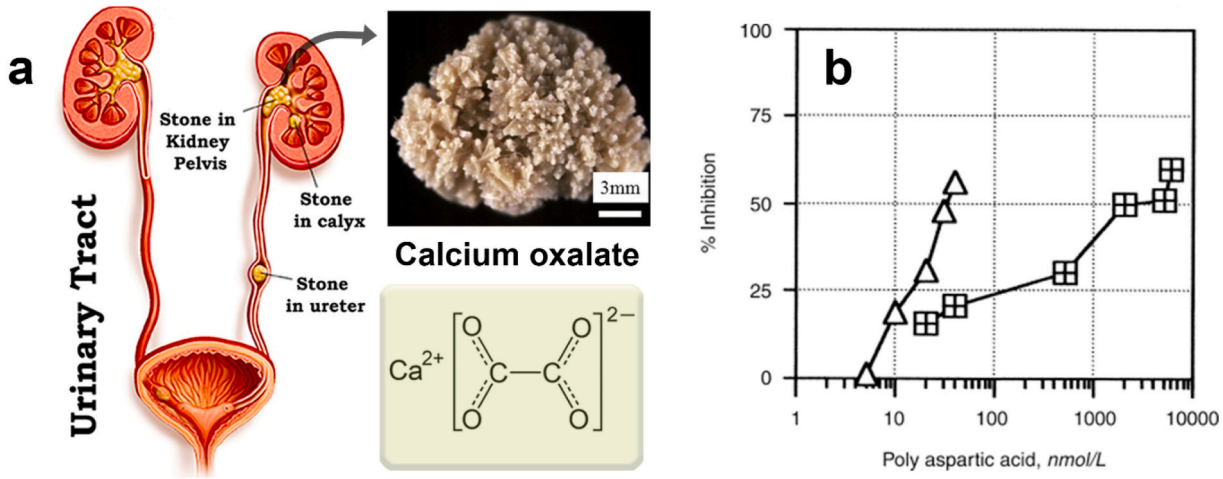

Fig. 11. Affinity of PASP to calcium oxalate and kidney stone. (a) As the kidney stone size increases, ureter blockage occurs, causing pain and variety of complications. Macroscopic observations of a type of kidney stones is shown [175]. (b) Inhibition of CaOx crystal growth (Δ) and aggregation (⊞) by PASP (Mw of 11 kDa). [133].

In conclusion, chelation therapy could be a viable strategy to treat kidney stones after addressing some important issues to ensure high efficacy of the treatment. Due to the abundance of calcium and other ions, premature action of the chelator is highly likely which highlights the importance of targeting the chelator to the calcifying site (i.e., urinary tract). Furthermore, selectivity towards calcium with minimal excretion of essential ions is highly preferable as well.

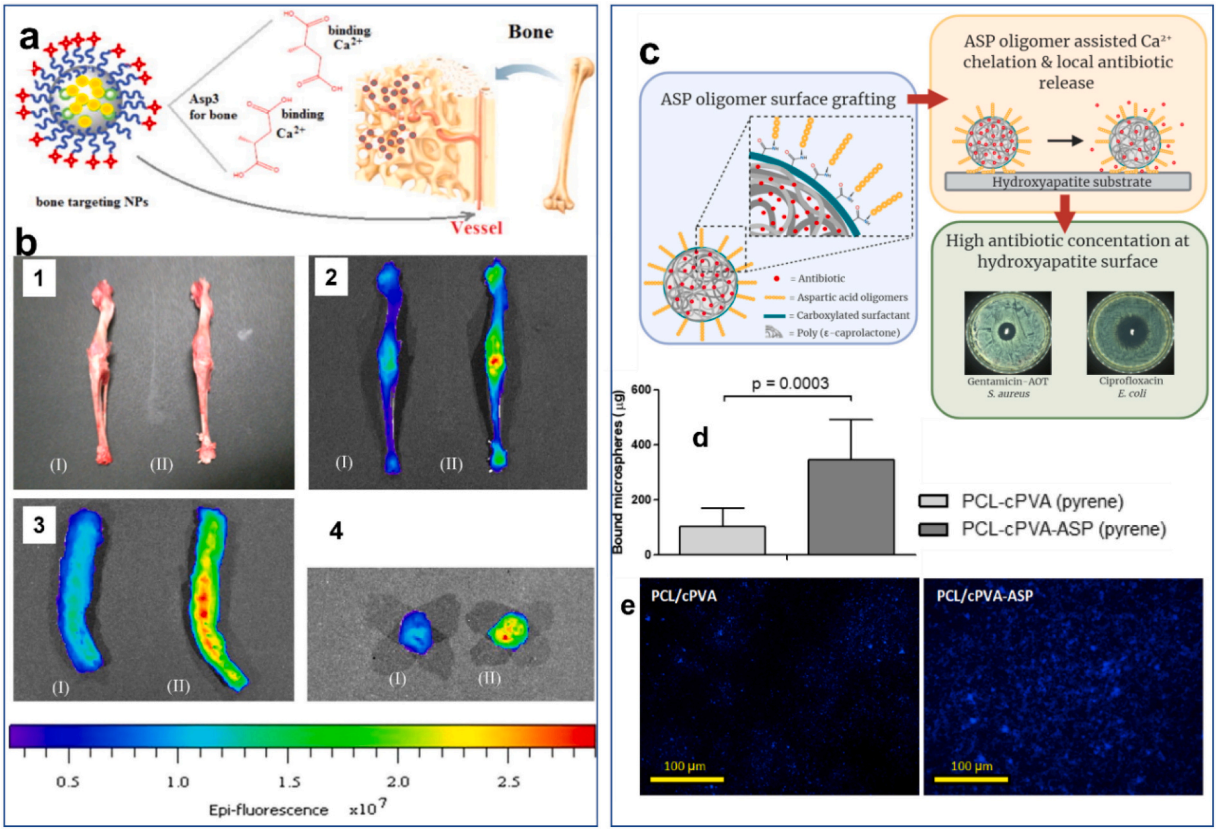

Fig. 12. Conjugation of PASP or oligomers of aspartic acid to nanoparticles improves their affinity to hydroxyapatite and bone. (a) Schematic representation of attachment of aspartic acid on the surface of PLGA-PEG NPs which can effectively bind to the surface of eroded bone. (b) Macroscopic photographs (1) and fluorescence images (2, 3, and 4) of different parts of the rats' bone taken 2 days after injection with (I) IR780/PLGA–PEG–OMe and (II) IR780/PLGA–PEG–Asp3 NPs . (1, and 2) are images of femur/tibia bone, while (3) and (4) are vertebrae bone, and cross-section of vertebrae bone, respectively. IR780 is a fluorescent dye that was loaded into PLGA-PEG NPs for tracking purpose [142]. (c) Schematic representation of conjugation of the antibiotic-loaded PCL particles with aspartic acid which improves its affinity to HAp surface and anti-bacterial activity. (d) Comparison of the amount of bound particles (μg) to HAp surface: ASP-conjugated particles showed significant improvement of binding compared to non-conjugated ones. (e) Microscopic images showing a significantly more intense blue color in aspartic acid-conjugated NPs. The blue color originates from pyrene which was loaded into the particles for tracking purpose [140]. (For interpretation of the references to color in this figure legend, the reader is referred to the web version of this article.)

4.9.2. Bone targeting ability of PASP

Calcium chelation of ASP and PASP which results in a high level of affinity with HAp -the main component of bone and dentin- has been used for targeting drug-loaded nanocarriers to bone [140–143]. Treating the diseases associated with bone is relatively difficult due to poor blood flow and therefore the importance of targeting the therapeutic agent is highlighted [144]. Thus, targeted delivery of bioactive agents could be of great importance. The targeting efficacy of aspartic acid groups to bone was exhibited in vitro and in vivo because its surface conjugation to PLGA-PEG NPs improved the accumulatio of the NPs in the bones (Fig. 12a, b) [142]. In another study, PASP was conjugated to paclitaxel-loaded liposomes, which improved bone targeting markedly, thereby enhancing treatment efficiency in metastatic tumor mouse models [145]. Fluorescent labelling of the particles showed their accumulation on the surface of eroded bone. The length of aspartic acid repeat units was optimized and found to provide efficient targeting in the range of 4–10 [146–148]. Another recent study also showed that conjugation of PASP on the surface of antibiotic-loaded poly(caprolactone) particles enhanced their attachment to HAp surfaces (Fig. 12c, d, e) [140]. Improved targeting of antibiotics is of great importance in the treatment of bone infection. Pyrene, as a fluorescent probe, was loaded into the particles to study the attachment onto the HAp surface [140]. The fluorescence intensity of HAp surface treated with PASP-conjugated particles was significantly higher than that with unconjugated particles. Fluorescence microscopic images from the HAP surfaces also verified improved attachment.

4.9.3. PASP for improving magnetic resonance imaging

As mentioned above, PASP could attach to the surface of NPs through chelation and stabilize them via electrostatic charge repulsion. Nanoparticles of [149,150] are widely used as MRI contrast agents [145,151–164], and PASP coatings has shown promising results in this regard [165]. PASP provides a high level of colloidal stability, leading to a high specific surface area which consequently enhances MRI contrast. PASP as compared to phospholipid-PEG was found to be more effective in improving the stability of manganese oxide NPs and thus their T_1 contrast [77]. The r_1 relaxivity of PASP-coated NPs were 3 to 5 times larger than that of phospholipid-PEG-coated NPs [77]. Marasini et al. [166] prepared dual modal T_1 and T_2 MRI contract agents (r_2/r_1 ratio = 2.8) by coating of PASP on gadolinium oxide (Gd_2O_3)NPs (2 nm). The r_1 and r_2 values of the coated NPs were around 5 and 10 times larger than the commercial gadolinium. In a recent investigation, immobilization of iron oxide NPs onto the PSI (precursor and anhydrous form of PASP) scaffold provided a long-term treatment with hyperthermic capability and suitable MRI contrast [167]. The hypothermic effect originated from the alternation of the magnetic field. PSI can be easily hydrolyzed in vivo to PASP and be eliminated through renal and bowel [167,168].

As an alternative to Gd-based MRI agents to address their nephrogenic systemic fibrosis-related issues, manganese oxide (MnO) NPs could be used as positive MRI agents [169]. Coating of MnO NPs with PASP grafted with RGD enhanced accumulation at the tumor [169]. Another study also compared PASP-PEG block copolymer-coated magnetite with a commercial MRI contrast agent (Resovist) [170]. Resovit is dextran-coated magnetite and was already approved for clinical use as a liver-specific MRI contrast agent. PASP-PEG-coated NPs showed a much better colloidal stability even at high ionic strength. While Resovit accumulated in the liver, PASP-PEG-coated magnetite NPs showed considerable negative enhancement of signal intensity in the tumor area of T2-weighted images [170]. Another study also showed accumulation of iron hydroxide NPs coated with PASP-PEG copolymer into tumor in-vivo, further strengthening its potential as a tumor-selective MRI contrast agent [171]. By spectroscopy, strong interaction of iron and PASP was also indicated, indicating effective coating of the NPs with the polymer [171]. Of note is that PASP has also significantly lowered the toxicity of iron oxide NPs [118] which could be attributed to iron chelation, as stated above.

4.10. Modification of PASP to improve its anti-scaling efficiency

Chemical modification of PASP by a variety of small molecules has been shown to further improve its chelation ability as summarized in Table 3. The precursor of PASP i.e., -poly(succinimide) (PSI)- can easily react with NH_2 groups under mild conditions at room temperature, opening a wide window for PASP functionalization (Fig. 13). As outlined in Table 3, the small molecules used for the reaction usually bear an amine group, otherwise, other conjugation approaches should be adopted. Following the reaction of PSI with the modifier, the polymer is subjected to alkali hydrolysis to convert the remnant succinimide groups to aspartic acid. This facile conjugation also enables the incorporation of fluorescent dyes into the chemical structure, which has subsequently facilitated the accurate determination of PASP concentration during or after water treatment [14,172]. In almost all studies listed in Table 3, a comparison between PASP and the modified PASP has been made in terms of scale inhibition, revealing higher efficacy of the latter. It is worthwhile to mention that making a comparison between the modifiers listed in the table is difficult as there is currently limited information in the literature on their calcium-binding affinity. Even with such data, the comparison would not be very accurate because the amine groups are converted to amide groups upon the ring-opening reaction with succinimide units. Nevertheless, if one considers the acidic strength (pKa) of the modifier as a criterion for comparison, sulfonic-based compounds (2-aminoethanesulfonic acid and sulfamic acid) should have higher calcium chelation effectivity compared to carboxylic- and phosphoric-based acids [14,37,173]. Such a comparison, however, would rule out amine-based chelators such as melamine as they are not acid.

One limitation of PASP is that it is not selective to some specific ions such as lead Pb^{2+}, and therefore its modification is necessary for such a purpose. For instance, L-cysteine-modified PASP showed a high affinity for removal of Pb^{2+} without significantly affecting other ions such as calcium, and iron [117]. Facile chemical modification of PASP, could be benefited in other areas such as chelation therapy where targeting could significantly enhance the treatment efficacy.

5. Conclusion and remarks

PASP is an anionic synthetic polypeptide and has exhibited excellent biocompatibility and biodegradability. Most studies have taken advantage of PASP's features, with little consideration to its ability to complex with metal ions. This review discussed different areas where the chelation ability of PASP in particular has thus far been exploited, in light of which the potential areas and future perspectives were also introduced. Industrially, PASP has been used mainly as a green antiscalant, and given the importance of environmental protection, its use is growing exponentially. PASP was shown to be an effective and edible stabilizer for preservation of wines. PASP has also exhibited excellent ability in stabilization of variety of colloidal systems that contain metal ions as a major surface constituent such as iron oxide nanoparticles, where excellent MRI contrast has been obtained. PASP chelation has also alleviated the toxicity of heavy metals in Zebrafish. Overall, the interest in PASP is exponentially growing due particularly to its complexation ability and is expected to be exploited in more areas. Our group is currently exploring the therapeutic efficacy of the polymer for different disorders. Hybrid organic/inorganic nanoparticles could be synthesized in-situ by taking advantage of ion chelation of PASP. In this regard, PASP hydrogels could be considered highly promising as ion reservoirs for NP formation. Furthermore, the development of PASP hydrogels could be highly beneficial for the removal of heavy metal ions from industrial wastewater. Through modification of PSI, chemical attachment of PASP onto a variety of membranes could be achieved for demineralization and removal of toxic heavy metals.

Table 3
Modification of PASP for improving anti-scaling efficiency against different minerals and chelation of heavy metals.

Modifying agent	Chemical structure of modifier	Mineral(s) studied	Improved Scale Inhibition efficiency	Fluorescence property	Corrosion Inhibition	Ref
Iminodiacetic acid	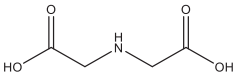	$CaCO_3$	Yes, due to the presence of two carboxylic acid groups of the modifier	n.d.	n.d.	[53]
Sulfamic acid With either histidine or arginine	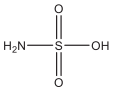 Sulfamic acid 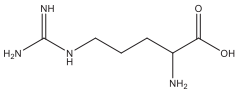 Arginine	$CaCO_3$, and $CaSO_4$	Yes	n.d.	Yes	[65]
Tyrosine, tryptophan and sulfamic acid	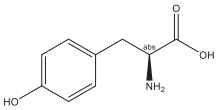 Tyrosine 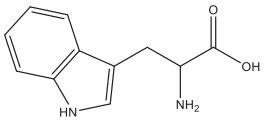 Tryptophan 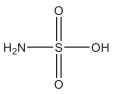 sulfamic acid	$CaSO_4$	Yes (more effective than PASP and commercially available scale inhibitors such as PAPEMP (phosphoric acid based) and JH-907 (acrylic acid based).	n.d.	n.d.	[148]
Carbazole (3-amino-9-ethyl carbazole) and hydroxyl (ethanolamine)	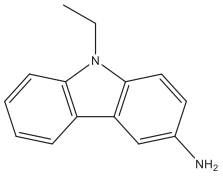 Carbazole(3-amino-9-ethyl carbazole) 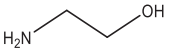 hydroxyl (ethanolamine)	CaP, $CaCO_3$	Yes	Yes, due to the presence of carbazole group	n.d.	[146]
Serine	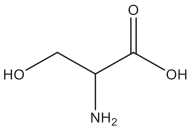	$CaCO_3$, $CaSO_4$, and CaP	Yes	n.d.	n.d.	[69]
2-aminoethanesulfonic acid	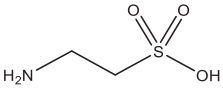	Seawater scale formation	Yes	n.d.	n.d.	[95]
Tryptophan, and taurine (2-aminoethanesulfonic acid)	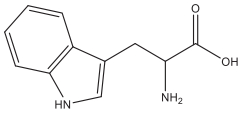 Tryptophan 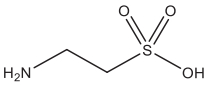 taurine (2-aminoethanesulfonic acid)	$CaSO_4$ and $CaCO_3$	Yes, due to sulfonic acid which is typically stronger than carboxylic acids.	Yes, due to indole group of tryptophan (emission peak at 390 nm)	n.d.	[11]
Aminobenzenesulfonic acid	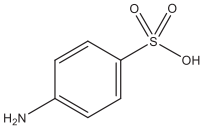	CaP and $CaCO_3$	n.d.	n.d.	n.d.	[76]
Urea	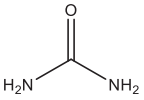	$CaCO_3$, $CaSO_4$ and CaP	Yes, due to acylamino group from urea which has lone pairs in the N atom.	n.d.	n.d.	[149]
5-amino orotic acid				n.d.	n.d.	[150]

(*continued on next page*)

Table 3 (*continued*)

Modifying agent	Chemical structure of modifier	Mineral(s) studied	Improved Scale Inhibition efficiency	Fluorescence property	Corrosion Inhibition	Ref
	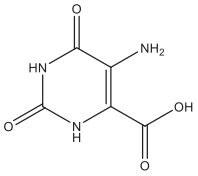	$CaCO_3$ and CaP	Yes, due to the presence of unsaturated six-membered ring lactam structure.			
Glycine	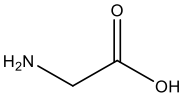	$CaSO_4$	n.d.	n.d.	Yes, for X-65 type carbon steel	[84]
N-(2,3-epoxylpropyl) carbazole and ethanolamine	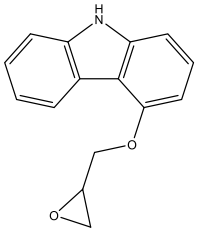 N-(2,3-epoxylpropyl) carbazole 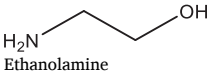 Ethanolamine	CaP and $CaCO_3$	The modified polymer showed better inhibition for CaP, while pure PASP was more effective for $CaCO_3$.	Yes, due to carbazole groups	n.d.	[151]
Tryptophan	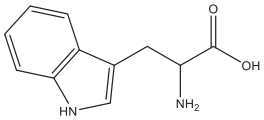	$CaSO_4$ and $CaCO_3$	Yes	n.d.	n.d.	[63]
2-amino-2-methyl-1,3-propanediol	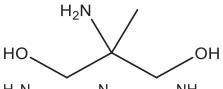	$CaCO_3$, $CaSO_4$, and CaP	Yes	n.d.	n.d.	[152]
Melamine	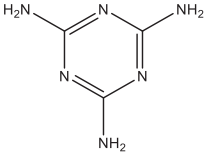	$CaCO_3$ and CaP	Yes, due to N-containing triazine ring from melamine	n.d.	n.d.	[77]
3-amino-1H-1,2,4-triazole-5-carboxylic acid hydrate	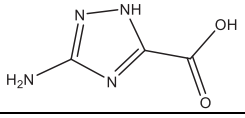	$CaCO_3$ and $CaSO_4$	Yes	n.d.	Yes	[64]

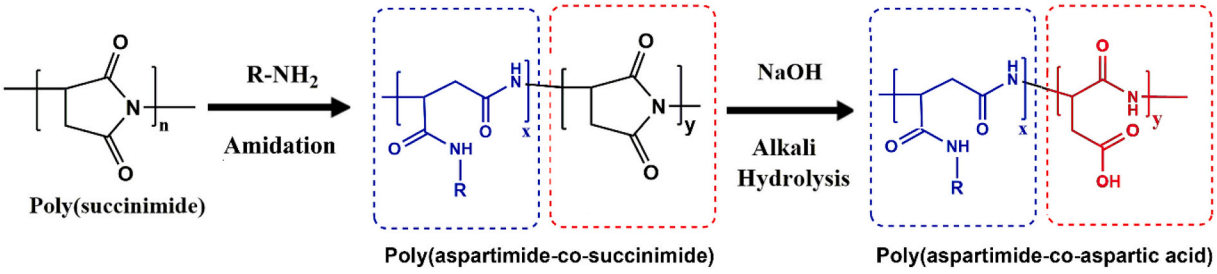

Fig. 13. Modification of PASP. The modification is typically carried out through amine-ring opening of PSI in the absence of catalyst at moderate temperatures. The partially hydrolyzed PSI is then hydrolyzed by an alkali to form poly(aspartimide-*co*-aspartic acid).

Funding

This work was supported by Australian National Health and Medical Research Council (HTT: APP1037310, APP1182347, APP2002827) and National Heart Foundation of Australia (HTT: 102761).

Declaration of competing interest

The authors declare that they have no known competing financial interests or personal relationships that could have appeared to influence the work reported in this paper.

References

[1] S. Robla, M.J. Alonso, N.S. Csaba, Polyaminoacid-based nanocarriers: A review of the latest candidates for oral drug delivery, Expert Opinion on Drug Delivery 17 (8) (2020) 1081–1092.
[2] A. Ganguly, K. Sharma, K. Majumder, Peptides as biopolymers—past, present, and future, in: Biopolymer-Based Formulations, Elsevier, 2020, pp. 87–104.

[3] T. Nakato, M. Yoshitake, K. Matsubara, M. Tomida, T. Kakuchi, Relationships between structure and properties of poly (aspartic acid) s, Macromolecules 31 (7) (1998) 2107–2113.
[4] K. Tabata, H. Abe, Y. Doi, Microbial degradation of poly (aspartic acid) by two isolated strains of pedobacter sp. And sphingomonas sp, Biomacromolecules 1 (2) (2000) 157–161.
[5] K. Tabata, M. Kajiyama, T. Hiraishi, H. Abe, I. Yamato, Y. Doi, Purification and characterization of poly (aspartic acid) hydrolase from sphingomonas sp. KT-1, Biomacromolecules 2 (4) (2001) 1155–1160.
[6] S.M. Thombre, B.D. Sarwade, Synthesis and biodegradability of polyaspartic acid: a critical review, J. Macromol. Sci. A 42 (9) (2005) 1299–1315.
[7] D. Juriga, K. Nagy, A. Jedlovszky-Hajdú, K. Perczel-Kovách, Y.M. Chen, G. Varga, M. Zrínyi, Biodegradation and osteosarcoma cell cultivation on poly (aspartic acid) based hydrogels, ACS Appl. Mater. Interfaces 8 (36) (2016) 23463–23476.
[8] H. Adelnia, I. Blakey, P.J. Little, H.T. Ta, Hydrogels based on poly (aspartic acid): synthesis and applications, Front. Chem. 7 (2019) 755.
[9] J.S. Lee, H.S. Park, Y.J. Kim, J.H. Kim, Hybrid double-network hydrogel based on poly (aspartic acid) and poly (acryl amide) with improved mechanical properties, J. Appl. Polym. Sci. 135 (9) (2018) 45925.
[10] S.K. Tarai, R. Bhaduri, S. Mukherjee, S. Mandal, S.C. Moi, Drug reservoir mechanism of Pt (II)-sulfur chelates based on pharmacokinetics of Pt (II) complex with thiols & thio-ethers: an experimental and theoretical approach, Inorg. Chim. Acta 517 (2021), 120202.
[11] H.-M. Yang, B.C. Oh, J.H. Kim, T. Ahn, H.-S. Nam, C.W. Park, J.-D.J.C. Kim, S. A. Physicochemical, E. Aspects, Multifunctional poly (aspartic acid) nanoparticles containing iron oxide nanocrystals and doxorubicin for simultaneous cancer diagnosis and therapy 391 (1–3) (2011) 208–215.
[12] S. Sattari, A.D. Tehrani, M. Adeli, F. Azarbani, Development of new nanostructure based on poly (aspartic acid)-g-amylose for targeted curcumin delivery using helical inclusion complex, J. Mol. Liq. 258 (2018) 18–26.
[13] D. Hasson, H. Shemer, A. Sher, State of the art of friendly "green" scale control inhibitors: a review article, Ind. Eng. Chem. Res. 50 (12) (2011) 7601–7607.
[14] Z. Shen, X. Zhi, P. Zhang, Preparation of fluorescent polyaspartic acid and evaluation of its scale inhibition for CaCO3 and CaSO4, Polym. Adv. Technol. 28 (3) (2017) 367–372.
[15] N.R. Jana, N. Erathodiyil, J. Jiang, J.Y. Ying, Cysteine-functionalized polyaspartic acid: a polymer for coating and bioconjugation of nanoparticles and quantum dots, Langmuir 26 (9) (2010) 6503–6507.
[16] V. Canuti, S. Cappelli, M. Picchi, B. Zanoni, P. Domizio, Screening Factors Affecting Potassium Polyaspartate and Carboxymethylcellulose Stability in Wine to Predict their Efficiency, Am. J. Enol. Viticul. (2019) ajev.2019.18077.
[17] D. Kołodyńska, Chitosan as an effective low-cost sorbent of heavy metal complexes with the polyaspartic acid, Chem. Eng. J. 173 (2) (2011) 520–529.
[18] P.-T. Ji, X.-L. Li, Y.-J. Peng, Y.-C. Zhang, P.-J. Tao, Effect of polyaspartic acid and different dosages of controlled-release fertilizers on nitrogen uptake, utilization, and yield of maize cultivars, Bioengineered 12 (1) (2021) 527–539.
[19] H.G. Yu, H.G. Ji, J.D. Kim, H.I. Jang, New anti-aging and anti-wrinkle material: properties and activities of nanoparticle containing poly (aspartic acid) derivatives, Journal of Nano Research, Trans Tech Publ (2019) 57–76.
[20] H. Adelnia, H.D.N. Tran, P.J. Little, I. Blakey, H.T. Ta, Poly(aspartic acid) in biomedical applications: from polymerization, modification, properties, degradation, and biocompatibility to applications, ACS Biomaterials Science & Engineering 7 (6) (2021) 2083–2105.
[21] P.S. Yavvari, A.K. Awasthi, A. Sharma, A. Bajaj, A. Srivastava, Emerging biomedical applications of polyaspartic acid-derived biodegradable polyelectrolytes and polyelectrolyte complexes, J. Mater. Chem. B 7 (13) (2019) 2102–2122.
[22] E. Jalalvandi, A. Shavandi, Polysuccinimide and its derivatives: degradable and water soluble polymers, Eur. Polym. J. 109 (2018) 43–54.
[23] G. Zhang, H. Yi, C. Bao, Stimuli-responsive poly (aspartamide) derivatives and their applications as drug carriers, Int. J. Mol. Sci. 22 (16) (2021) 8817.
[24] P. Das, N.R. Jana, Biomedical applications of functional polyaspartamide-based materials, ACS Appl. Polym. Mater. 3 (10) (2021) 4791–4811.
[25] G. Boehmke, Polyaspartic acid from maleic acid and ammonia, in: Google Patents, 1989.
[26] S.K. Wolk, G. Swift, Y.H. Paik, K.M. Yocom, R.L. Smith, E.S. Simon, One-and two-dimensional nuclear magnetic resonance characterization of poly (aspartic acid) prepared by thermal polymerization of L-aspartic acid, Macromolecules 27 (26) (1994) 7613–7620.
[27] K.C. Low, A. Wheeler, L.P. Koskan, Commercial poly (aspartic acid) and its uses, Adv. Chem. Ser. 248 (1996) 99–112.
[28] J.-P. Zeng, F.-H. Wang, X.-D. Gong, Molecular dynamics simulation of the interaction between polyaspartic acid and calcium carbonate, Mol. Simul. 39 (3) (2013) 169–175.
[29] T. Nakato, M. Yoshitake, K. Matsubara, M. Tomida, T. Kakuchi, Relationships between structure and properties of poly(aspartic acid)s, Macromolecules 31 (7) (1998) 2107–2113.
[30] K. Rubini, E. Boanini, A. Bigi, Role of aspartic and polyaspartic acid on the synthesis and hydrolysis of brushite, J. Funct. Biomater. 10 (1) (2019) 11.
[31] J. Wesson, E. Worcester, Formation of hydrated calcium oxalates in the presence of poly-L-aspartic acid, Scanning Microsc. 10 (2) (1996) 415–423, 423–4.
[32] S. Guo, M.D. Ward, J.A. Wesson, Direct visualization of calcium oxalate monohydrate crystallization and dissolution with atomic force microscopy and the role of polymeric additives, Langmuir 18 (11) (2002) 4284–4291.
[33] K. Burns, Y.-T. Wu, C.S. Grant, Mechanisms of calcite dissolution using environmentally benign polyaspartic acid: A rotating disk study, Langmuir 19 (14) (2003) 5669–5679.
[34] T. Rabizadeh, D.J. Morgan, C.L. Peacock, L.G. Benning, Effectiveness of green additives vs poly (acrylic acid) in inhibiting calcium sulfate dihydrate crystallization, Ind. Eng. Chem. Res. 58 (4) (2019) 1561–1569.
[35] H. Adelnia, R. Ensandoost, S. Shebbrin Moonshi, J.N. Gavgani, E.I. Vasafi, H. T. Ta, Freeze/thawed polyvinyl alcohol hydrogels: Present, past and future, European Polymer Journal 164 (2022) 110974.
[36] S.E. Alavi, M.K.M. Esfahani, A. Raza, H. Adelnia, H.E. Shahmabadi, PEG-grafted liposomes for enhanced antibacterial and antibiotic activities: An in vivo study, NanoImpact 25 (2022) 100384.
[37] S.M. Molaei, H. Adelnia, A.M. Seif, J. Nasrollah Gavgani, Sulfonate-functionalized polyacrylonitrile-based nanoparticles; synthesis, and conversion to pH-sensitive nanogels, Colloid Polym. Sci. 297 (9) (2019) 1245–1253.
[38] H. Kimoto, A. Yanagisawa, A. Asano, C. Nakazawa, E. Shinohara, T. Kurotsu, Voltammetric evaluation on poly α-aspartic acid-zinc ion complex in the helix-coil transitionpH region, Analytical Sciences 27 (11) (2011).
[39] Y.-T. Wu, C. Grant, Effect of chelation chemistry of sodium polyaspartate on the dissolution of calcite, Langmuir 18 (18) (2002) 6813–6820.
[40] H. Adelnia, S. Pourmahdian, Soap-free emulsion polymerization of poly (methyl methacrylate-co-butyl acrylate): effects of anionic comonomers and methanol on the different characteristics of the latexes, Colloid Polym. Sci. 292 (1) (2014) 197–205.
[41] H. Adelnia, J.N. Gavgani, H. Riazi, H.C. Bidsorkhi, Transition behavior, surface characteristics and film formation of functionalized poly (methyl methacrylate-co-butyl acrylate) particles, Prog. Org. Coat. 77 (11) (2014) 1826–1833.
[42] R. Fu, D. Wen, X. Xia, W. Zhang, Y. Gu, Electrokinetic remediation of chromium (Cr)-contaminated soil with citric acid (CA) and polyaspartic acid (PASP) as electrolytes, Chem. Eng. J. 316 (2017) 601–608.
[43] E. Gutierrez, T.C. Miller, J.R. Gonzalez-Redondo, J.A. Holcombe, Characterization of immobilized poly-l-aspartate as a metal chelator, Environ. Sci. Technol. 33 (10) (1999) 1664–1670.
[44] G. Berthon, Handbook of Metal-ligand Interactions in Biological Fluids, Marcel Dekker, 1995.
[45] J.P. Glusker, Structural aspects of metal liganding to functional groups in proteins, Adv. Protein Chem. 42 (1991) 1–76.
[46] L. Malachowski, J.A. Holcombe, Comparison of immobilized poly-L-aspartic acid and poly-l-glutamic acid for chelation of metal cations, Anal. Chim. Acta 517 (1–2) (2004) 187–193.
[47] J.L. Stair, J.A. Holcombe, Metal binding characterization and conformational studies using Raman microscopy of resin-bound poly (aspartic acid), Anal. Chem. 79 (5) (2007) 1999–2006.
[48] M. Schweinsberg, W. Hater, J. Verdes, New stable biodegradable scale inhibitor formulations for cooling water: development and field tests, in: 64th International Water Conference, Pittsburgh, PA, 2003.
[49] B. Njegic-Dzakula, L. Brecevic, G. Falini, D. Kralj, Calcite crystal growth kinetics in the presence of charged synthetic polypeptides, Crystal Growth Des. 9 (5) (2009) 2425–2434.
[50] S.L. Wolf, K. Jähme, D. Gebauer, Synergy of Mg 2+ and poly (aspartic acid) in additive-controlled calcium carbonate precipitation, CrystEngComm 17 (36) (2015) 6857–6862.
[51] G. Gwak, B. Jung, S. Han, S. Hong, Evaluation of poly (aspartic acid sodium salt) as a draw solute for forward osmosis, Water Res. 80 (2015) 294–305.
[52] I.R. Collins, Surface electrical properties of barium sulfate modified by adsorption of poly α, β aspartic acid, J. Colloid Interface Sci. 212 (2) (1999) 535–544.
[53] D. Liu, W. Dong, F. Li, F. Hui, J. Lédion, Comparative performance of polyepoxysuccinic acid and polyaspartic acid on scaling inhibition by static and rapid controlled precipitation methods, Desalination 304 (2012) 1–10.
[54] R. Chang, S. Kim, S. Lee, S. Choi, M. Kim, Y. Park, Calcium carbonate precipitation for CO2 storage and utilization: a review of the carbonate crystallization and polymorphism, Front. Energy Res. 5 (2017) 17.
[55] R. Ševčík, P. Šašek, A. Viani, Physical and nanomechanical properties of the synthetic anhydrous crystalline CaCO 3 polymorphs: vaterite, aragonite and calcite, J. Mater. Sci. 53 (6) (2018) 4022–4033.
[56] E.O. Ohimor, O.E. Anigboro, C. Anih, Performance Evaluation of Biodegradable Oilfield Scale Inhibitors for Calcium Carbonate Scales, 2019.
[57] S. Eichinger, R. Boch, A. Leis, A. Baldermann, G. Domberger, C. Schwab, M. Dietzel, Green inhibitors reduce unwanted calcium carbonate precipitation: Implications for technical settings, Water Res. 208 (2022), 117850.
[58] Z. Zou, L. Bertinetti, Y. Politi, P. Fratzl, W.J. Habraken, Control of Polymorph Selection in Amorphous Calcium Carbonate Crystallization by Poly (Aspartic Acid): Two Different Mechanisms, Small 13 (21) (2017) 1603100.
[59] A. Martinod, A. Neville, M. Euvrad, K. Sorbie, Electrodeposition of a calcareous layer: Effects of green inhibitors, Chem. Eng. Sci. 64 (10) (2009) 2413–2421.
[60] X. Guo, X. Zhao, Y. Xu, P. Zhang, Y. Cheng, Y. Xu, The synthesis of polyaspartic acid derivative PASP-Im and investigation of its scale inhibition performance and mechanism in industrial circulating water, RSC Adv. 10 (55) (2020) 33595–33601.
[61] E. Dalas, P. Malkaj, Z. Vasileiou, D. Kanellopoulou, The effect of Leucine on the crystal growth of calcium phosphate, J. Mater. Sci. Mater. Med. 19 (1) (2008) 277–282.
[62] D.V. Krogstad, D. Wang, S. Lin-Gibson, Polyaspartic acid concentration controls the rate of calcium phosphate nanorod formation in high concentration systems, Biomacromolecules 18 (10) (2017) 3106–3113.

[63] A. Bigi, B. Bracci, S. Panzavolta, M. Iliescu, M. Plouet-Richard, J. Werckmann, D. Cam, Morphological and structural modifications of octacalcium phosphate induced by poly-L-aspartate, Cryst. Growth Des. 4 (1) (2004) 141–146.
[64] F. Poumier, P. Schaad, Y. Haikel, J. Voegel, P. Gramain, Dissolution of synthetic hydroxyapatite in the presence of acidic polypeptides, Journal of Biomedical Materials Research: An Official Journal of The Society for Biomaterials, The Japanese Society for Biomaterials, and The Australian Society for Biomaterials 45 (2) (1999) 92–99.
[65] F. Littlejohn, A.E. Sáez, C.S. Grant, Use of sodium polyaspartate for the removal of hydroxyapatite/brushite deposits from stainless steel tubing, Ind. Eng. Chem. Res. 37 (7) (1998) 2691–2700.
[66] F. Littlejohn, C.S. Grant, Y.L. Wong, A.E. Sáez, Effect of poly (aspartic acid) on the removal rates of brushite deposits from stainless steel tubing in turbulent flow, Ind. Eng. Chem. Res. 41 (18) (2002) 4576–4584.
[67] M. Othmani, A. Aissa, H. Bachoua, M. Debbabi, Surface modification of calcium–copper hydroxyapatites using polyaspartic acid, Appl. Surf. Sci. 264 (2013) 886–891.
[68] A.G. Dickson, C. Goyet, Handbookof Methods for the Analysis of the Various Parameters of the Carbon DioxideSystem in Sea Water. Version 2, Oak Ridge National Lab, TN (United States), 1994.
[69] X. Sun, J. Zhang, C. Yin, J. Zhang, J. Han, Poly (aspartic acid)–tryptophan grafted copolymer and its scale-inhibition performance, J. Appl. Polym. Sci. 132 (45) (2015).
[70] B. Zhang, D. Zhou, X. Lv, Y. Xu, Y. Cui, Synthesis of polyaspartic acid/3-amino-1H-1, 2, 4-triazole-5-carboxylic acid hydrate graft copolymer and evaluation of its corrosion inhibition and scale inhibition performance, Desalination 327 (2013) 32–38.
[71] L. Zhao, Y. Zhou, Q. Yao, Y. Wang, S. Ge, X. Liu, Calcium scale inhibition of stimulated oilfield produced water using polyaspartic acid/ aminomethanesulfonic acid, ChemistrySelect 6 (15) (2021) 3692–3701.
[72] M.F. Mady, A. Rehman, M.A. Kelland, Synthesis and Study of Modified Polyaspartic Acid Coupled Phosphonate and Sulfonate Moieties As Green Oilfield Scale Inhibitors, Ind. Eng. Chem. Res. 60 (23) (2021) 8331–8339.
[73] Y. Cheng, X. Guo, X. Zhao, Y. Wu, Z. Cao, Y. Cai, Y. Xu, Nanosilica modified with polyaspartic acid as an industrial circulating water scale inhibitor, npj CleanWater 4 (1) (2021) 1–8.
[74] J. Chen, L. Xu, J. Han, M. Su, Q. Wu, Synthesis of modified polyaspartic acid and evaluation of its scale inhibition and dispersion capacity, Desalination 358 (2015) 42–48.
[75] A. Golabdar, H. Adelnia, N. Moshtzan, J. Nasrollah Gavgani, H. Izadi-Vasafi, Anti-bacterial poly (vinyl alcohol) nanocomposite hydrogels reinforced with in situ synthesized silver nanoparticles, Polym. Compos. 40 (4) (2019) 1322–1328.
[76] X. Wang, B.I. Lee, L. Mann, Dispersion of barium titanate with polyaspartic acid in aqueous media, Colloids Surf. A Physicochem. Eng. Asp. 202 (1) (2002) 71–80.
[77] R. Xing, F. Zhang, J. Xie, M. Aronova, G. Zhang, N. Guo, X. Huang, X. Sun, G. Liu, L.H. Bryant, Polyaspartic acid coated manganese oxide nanoparticles for efficient liver MRI, Nanoscale 3 (12) (2011) 4943–4945.
[78] S.V. Khandekar, M. Kulkarni, P.V. Devarajan, Polyaspartic acid functionalized gold nanoparticles for tumor targeted doxorubicin delivery, J. Biomed. Nanotechnol. 10 (1) (2014) 143–153.
[79] D. Barczikai, V. Kacsari, J. Domokos, D. Szabo, A. Jedlovszky-Hajdu, Interaction of silver nanoparticle and commonly used anti-inflammatory drug within a poly (amino acid) derivative fibrous mesh, J. Mol. Liq. 322 (2021), 114575.
[80] H.S. Kang, S.R. Yang, J.-D. Kim, S.-H. Han, I.-S. Chang, Effects of grafted alkyl groups on aggregation behavior of amphiphilic poly (aspartic acid), Langmuir 17 (24) (2001) 7501–7506.
[81] T. Nakato, M. Tomida, M. Suwa, Y. Morishima, A. Kusuno, T. Kakuchi, Preparation and characterization of dodecylamine-modified poly (aspartic acid) as a biodegradable water-soluble polymeric material, Polym. Bull. 44 (4) (2000) 385–391.
[82] Y. Xu, L. Wang, L. Zhao, Y. Cui, Synthesis of polyaspartic acid–aminobenzenesulfonic acid grafted copolymer and its scale inhibition performance and dispersion capacity, Water Sci. Technol. 64 (2) (2011) 423–430.
[83] Y. Xu, L. Zhao, L. Wang, S. Xu, Y. Cui, Synthesis of polyaspartic acid–melamine grafted copolymer and evaluation of its scale inhibition performance and dispersion capacity for ferric oxide, Desalination 286 (2012) 285–289.
[84] V. Canuti, S. Cappelli, M. Picchi, B. Zanoni, P. Domizio, Effects of high temperatures on the efficacy of potassium polyaspartate for tartaric stabilization in wines, Am. J. Enol. Vitic. 70 (3) (2019) 332–337.
[85] A. Bosso, R. Lopez, L. Panero, S. Motta, M. Petrozziello, A. Asproudi, M. Guaita, Useof Polyaspartates for the Tartaric Stabilisation of White and Red Wines and SideEffects on Wine Characteristics, 2020.
[86] A. Bosso, L. Panero, M. Petrozziello, M. Sollazzo, A. Asproudi, S. Motta, M. Guaita, Use of polyaspartate as inhibitor of tartaric precipitations in wines, Food Chem. 185 (2015) 1–6.
[87] R. Eder, M. Willach, M. Strauss, C. Philipp, Efficient tartaric stabilisation of white wine with potassium polyaspartate, in: BIO Web of Conferences, EDP Sciences, 2019.
[88] Y. Gao, L. Ward, L. Fan, H. Li, Z. Liu, A study of the use of polyaspartic acid derivative composite for the corrosion inhibition of carbon steel in a seawater environment, J. Mol. Liq. 294 (2019), 111634.
[89] L. Fu, J. Lv, L. Zhou, Z. Li, M. Tang, J. Li, Study on corrosion and scale inhibition mechanism of polyaspartic acid grafted β-cyclodextrin, Mater. Lett. 264 (2020), 127276.
[90] M. Migahed, S. Rashwan, M. Kamel, R. Habib, Synthesis, characterization of polyaspartic acid-glycine adduct and evaluation of their performance as scale and corrosion inhibitor in desalination water plants, J. Mol. Liq. 224 (2016) 849–858.
[91] C. Chai, Y. Xu, D. Li, X. Zhao, Y. Xu, L. Zhang, Y. Wu, Cysteamine modified polyaspartic acid as a new class of green corrosion inhibitor for mild steel in sulfuric acid medium: synthesis, electrochemical, surface study and theoretical calculation, Progress in Organic Coatings 129 (2019) 159–170.
[92] C. Wang, J. Chen, J. Han, C. Wang, B. Hu, Enhanced corrosion inhibition performance of novel modified polyaspartic acid on carbon steel in HCl solution, J. Alloys Compd. 771 (2019) 736–746.
[93] R. Cui, N. Gu, C. Li, Polyaspartic acid as a green corrosion inhibitor for carbon steel, Mater. Corros. 62 (4) (2011) 362–369.
[94] L. Yang, Y. Li, B. Qian, B. Hou, Polyaspartic acid as a corrosion inhibitor for WE43 magnesium alloy, J. Magnesium Alloys 3 (1) (2015) 47–51.
[95] A. Zeino, I. Abdulazeez, M. Khaled, M.W. Jawich, I.B. Obot, Mechanistic study of polyaspartic acid (PASP) as eco-friendly corrosion inhibitor on mild steel in 3% NaCl aerated solution, J. Mol. Liq. 250 (2018) 50–62.
[96] C. Chai, Y. Xu, Y. Xu, S. Liu, L. Zhang, Dopamine-modified polyaspartic acid as a green corrosion inhibitor for mild steel in acid solution, Eur. Polym. J. 137 (2020), 109946.
[97] M. Vatankhah-Varnosfaderani, X. Hu, Q. Li, H. Adelnia, M. Ina, S.S. Sheiko, Universal coatings based on zwitterionic–dopamine copolymer microgels, ACS Appl. Mater. Interfaces 10 (24) (2018) 20869–20875.
[98] M. Vatankhah-Varnoosfaderani, M. Ina, H. Adelnia, Q. Li, A.P. Zhushma, L. J. Hall, S.S. Sheiko, Well-defined zwitterionic microgels: synthesis and application as acid-resistant microreactors, Macromolecules 49 (19) (2016) 7204–7210.
[99] G. Khan, W.J. Basirun, S.N. Kazi, P. Ahmed, L. Magaji, S.M. Ahmed, G.M. Khan, M.A. Rehman, A.B.B.M. Badry, Electrochemical investigation on the corrosion inhibition of mild steel by Quinazoline Schiff base compounds in hydrochloric acid solution, J. Colloid Interface Sci. 502 (2017) 134–145.
[100] A. Kumar, M. Trivedi, R.K. Sharma, G. Singh, Synthetic, spectral and structural studies of a Schiff base and its anticorrosive activity on mild steel in H 2 SO 4, New J. Chem. 41 (16) (2017) 8459–8468.
[101] Y. Gao, L. Fan, L. Ward, Z. Liu, Synthesis of polyaspartic acid derivative and evaluation of its corrosion and scale inhibition performance in seawater utilization, Desalination 365 (2015) 220–226.
[102] D. Wang, J. Xu, J. Wang, W. Hu, Preparation and corrosion resistance of polyaspartic acid-zinc self-assembled film on carbon steel surface, Colloids Surf. A Physicochem. Eng. Asp. 608 (2021), 125615.
[103] B.K. Pramanik, Y. Gao, L. Fan, F.A. Roddick, Z. Liu, Antiscaling effect of polyaspartic acid and its derivative for RO membranes used for saline wastewater and brackish water desalination, Desalination 404 (2017) 224–229.
[104] D. Leštan, C.-L. Luo, X.-D. Li, The use of chelating agents in the remediation of metal-contaminated soils: a review, Environ. Pollut. 153 (1) (2008) 3–13.
[105] T. Liu, R. Wang, H. Cao, A. Lin, Polyaspartic acid alleviates heavy metal toxicity in zebrafish (Danio rerio), Chem. Ecol. 33 (7) (2017) 684–693.
[106] M.K. Nayunigari, S.K. Gupta, V. Kokkarachedu, K. Kanny, F. Bux, Development of anti-scale poly (aspartic acid–citric acid) dual polymer systems for water treatment, Environ. Technol. 35 (23) (2014) 2903–2909.
[107] H. Wang, B. Zhao, L. Wang, Adsorption/desorption performance of Pb2+ and Cd2 + with super adsorption capacity of PASP/CMS hydrogel, Water Sci. Tech. 84 (1) (2021) 43–54.
[108] X.J. Chen, J.C. Cai, Z.H. Zhang, L.J. Liu, G.L. Yang, Investigation of removal of Pb (II) and Hg (II) by a novel cross-linked chitosan-poly (aspartic acid) chelating resin containing disulfide bond, Colloid Polym. Sci. 292 (9) (2014) 2157–2172.
[109] J.-H. Seo, S.J. Park, S.H. Um, S.W. Nam, Y.J. Kim, J.-H. Kim, Swelling and metal-ion adsorption properties of dopamine-conjugated polyaspartate hydrogel, J. Polym. Environ. 23 (1) (2015) 90–96.
[110] F. Zhang, J. Teng, D. Han, L. Wu, W. Hou, Preparationof Hydrogel Based on Poplar Cellulose and Its Removal of Cd (II) From AqueousSolution, 2022.
[111] C.-Y. Chen, M.-S. Lin, K.-R. Hsu, Recovery of Cu (II) and Cd (II) by a chelating resin containing aspartate groups, J. Hazard. Mater. 152 (3) (2008) 986–993.
[112] W. Yang, J.J. Gooding, D.B. Hibbert, Redox voltammetry of sub-parts per billion levels of Cu2+ at polyaspartate-modified gold electrodes, Analyst 126 (9) (2001) 1573–1577.
[113] C. Zhang, H. Li, Q. Yu, L. Jia, L.Y. Wan, Poly (aspartic acid) electrospun nanofiber hydrogel membrane-based reusable colorimetric sensor for Cu (II) and Fe (III) detection, ACS Omega 4 (11) (2019) 14633–14639.
[114] D. Mogopodi, N. Torto, Enhancing microdialysis recovery of metal ions by incorporating poly-L-aspartic acid and poly-L-histidine in the perfusion liquid, Anal. Chim. Acta 482 (1) (2003) 91–97.
[115] D. Mogopodi, N. Torto, Maximising metal ions flux across a microdialysis membrane by incorporating poly-l-aspartic acid, poly-l-histidine, 8-hydroxyquinoline and ethylenediaminetetraacetic acid in the perfusion liquid, Anal. Chim. Acta 534 (2) (2005) 239–246.
[116] N. Torto, D. Mogopodi, Opportunities in microdialysis sampling of metal ions, TrAC Trends Anal. Chem. 23 (2) (2004) 109–115.
[117] L. Li, J. Wu, M. Zhao, Y. Wang, H. Zhang, X. Zhang, L. Gui, J. Liu, N. Mair, S. Peng, Poly-α, β-dl-Aspartyl-l-cysteine: a novel nanomaterial having a porous structure, special complexation capability for Pb (II), and selectivity of removing Pb (II), Chem. Res. Toxicol. 25 (9) (2012) 1948–1954.
[118] S. Wan, J. Huang, M. Guo, H. Zhang, Y. Cao, H. Yan, K. Liu, Biocompatible superparamagnetic iron oxide nanoparticle dispersions stabilized with poly (ethylene glycol)–oligo (aspartic acid) hybrids, J. Biomed. Mater. Res. A 80 (4) (2007) 946–954.

[119] Z. Varga, K. Molnár, V. Torma, M. Zrínyi, Kinetics of volume change of poly (succinimide) gels during hydrolysis and swelling, Phys. Chem. Chem. Phys. 12 (39) (2010) 12670–12675.
[120] E. Krisch, L. Messager, B. Gyarmati, V. Ravaine, A. Szilágyi, Redox-and pH-Responsive Nanogels Based on Thiolated Poly (aspartic acid), Macromol. Mater. Eng. 301 (3) (2016) 260–266.
[121] M. Zrinyi, T. Gyenes, D. Juriga, J.-H. Kim, Volume change of double cross-linked poly (aspartic acid) hydrogels induced by cleavage of one of the crosslinks, Acta Biomater. 9 (2) (2013) 5122–5131.
[122] D. Juriga, E.E. Kalman, K. Toth, D. Barczikai, D. Szöllősi, A. Földes, G. Varga, M. Zrinyi, A. Jedlovszky-Hajdu, K.S. Nagy, Analysis of three-dimensional cell migration in dopamine-modified poly (aspartic acid)-based hydrogels, Gels 8 (2) (2022) 65.
[123] A. Mammadova, B. Gyarmati, K. Sárdi, A. Paudics, Z. Varga, A. Szilágyi, Thiolated cationic poly(aspartamides) with side group dependent gelation properties for the delivery of anionic polyelectrolytes, J. Mater. Chem. B 10 (31) (2022) 5946–5957.
[124] L. Sheng, I. Leshchyns'ka, V. Sytnyk, Cell adhesion and intracellular calcium signaling in neurons, Cell Communication and Signaling 11 (1) (2013) 1–13.
[125] C.R. Reczek, N.S. Chandel, The two faces of reactive oxygen species in cancer, Annu. Rev. Cancer Biol. 1 (2017) 79–98.
[126] M. Jung, C. Mertens, E. Tomat, B. Brüne, Iron as a central player and promising target in cancer progression, Int. J. Mol. Sci. 20 (2) (2019) 273.
[127] H. Shiraga, W. Min, W. VanDusen, M. Clayman, D. Miner, C. Terrell, J. Sherbotie, J. Foreman, C. Przysiecki, E. Neilson, Inhibition of calcium oxalate crystal growth in vitro by uropontin: another member of the aspartic acid-rich protein superfamily, Proceedings of the National Academy of Sciences 89 (1) (1992) 426–430.
[128] L. Wang, S.R. Qiu, W. Zachowicz, X. Guan, J.J. DeYoreo, G.H. Nancollas, J. R. Hoyer, Modulation of calcium oxalate crystallization by linear aspartic acid-rich peptides, Langmuir 22 (17) (2006) 7279–7285.
[129] S.A. Steitz, M.Y. Speer, M.D. McKee, L. Liaw, M. Almeida, H. Yang, C.M. Giachelli, Osteopontin inhibits mineral deposition and promotes regression of ectopic calcification, The American journal of pathology 161 (6) (2002) 2035–2046.
[130] N.J. Paloian, E.M. Leaf, C.M. Giachelli, Osteopontin protects against high phosphate-induced nephrocalcinosis and vascular calcification, Kidney Int. 89 (5) (2016) 1027–1036.
[131] J.R. Asplin, D. Arsenault, J.H. Parks, F.L. Coe, J.R. Hoyer, Contribution of human uropontin to inhibition of calcium oxalate crystallization, Kidney Int. 53 (1) (1998) 194–199.
[132] M.A. Icer, M. Gezmen-Karadag, The multiple functions and mechanisms of osteopontin, Clin. Biochem. 59 (2018) 17–24.
[133] J.R. Hoyer, J.R. Asplin, L. Otvos Jr., Phosphorylated osteopontin peptides suppress crystallization by inhibiting the growth of calcium oxalate crystals, Kidney Int. 60 (1) (2001) 77–82.
[134] H. Ito, F. Coe, Acidic peptide and polyribonucleotide crystal growth inhibitors in human urine, Am. J. Physiol. Renal Physiol. 233 (5) (1977) F455–F463.
[135] E.M. Worcester, S.S. Blumenthal, A.M. Beshensky, D.L. Lewand, The calcium oxalate crystal growth inhibitor protein produced by mouse kidney cortical cells in culture is osteopontin, J. Bone Miner. Res. 7 (9) (1992) 1029–1036.
[136] J.D. Rimer, A.M. Kolbach-Mandel, M.D. Ward, J.A. Wesson, The role of macromolecules in the formation of kidney stones, Urolithiasis 45 (1) (2017) 57–74.
[137] X. Sheng, M.D. Ward, J.A. Wesson, Adhesion between molecules and calcium oxalate crystals: critical interactions in kidney stone formation, J. Am. Chem. Soc. 125 (10) (2003) 2854–2855.
[138] M.A. Kelland, M.F. Mady, R. Lima-Eriksen, Kidney stone prevention: dynamic testing of edible calcium oxalate scale inhibitors, Cryst. Growth Des. 18 (12) (2018) 7441–7450.
[139] W. Min, H. Shiraga, C. Chalko, S. Goldfarb, G.G. Krishna, J.R. Hoyer, Quantitative studies of human urinary excretion of uropontin, Kidney Int. 53 (1) (1998) 189–193.
[140] S.G. Rotman, T.F. Moriarty, B. Nottelet, D.W. Grijpma, D. Eglin, O. Guillaume, Poly (aspartic acid) functionalized poly (ε-caprolactone) microspheres with enhanced hydroxyapatite affinity as bone targeting antibiotic carriers, Pharmaceutics 12 (9) (2020) 885.
[141] A. Lotsari, A.K. Rajasekharan, M. Halvarsson, M. Andersson, Transformation of amorphous calcium phosphate to bone-like apatite, Nat. Commun. 9 (1) (2018) 1–11.
[142] Y.-C. Fu, T.-F. Fu, H.-J. Wang, C.-W. Lin, G.-H. Lee, S.-C. Wu, C.-K. Wang, Aspartic acid-based modified PLGA–PEG nanoparticles for bone targeting: In vitro and in vivo evaluation, Acta Biomater. 10 (11) (2014) 4583–4596.
[143] T. Jiang, X. Yu, E.J. Carbone, C. Nelson, H.M. Kan, K.W.-H. Lo, Poly aspartic acid peptide-linked PLGA based nanoscale particles: potential for bone-targeting drug delivery applications, Int. J. Pharm. 475 (1–2) (2014) 547–557.
[144] D.B. Chastain, A. Davis, Treatment of chronic osteomyelitis with multidose oritavancin: a case series and literature review, Int. J. Antimicrob. Agents 53 (4) (2019) 429–434.
[145] S. Yamashita, H. Katsumi, N. Hibino, Y. Isobe, Y. Yagi, Y. Tanaka, S. Yamada, C. Naito, A. Yamamoto, Development of PEGylated aspartic acid-modified liposome as a bone-targeting carrier for the delivery of paclitaxel and treatment of bone metastasis, Biomaterials 154 (2018) 74–85.
[146] K. Ogawa, A. Ishizaki, K. Takai, Y. Kitamura, T. Kiwada, K. Shiba, A. Odani, Development of novel radiogallium-labeled bone imaging agents using oligo-aspartic acid peptides as carriers, PLoS One 8 (12) (2013), e84335.
[147] D. Wang, S.C. Miller, L.S. Shlyakhtenko, A.M. Portillo, X.-M. Liu, K. Papangkorn, P. Kopecková, Y. Lyubchenko, W.I. Higuchi, J. Kopeček, Osteotropic peptide that differentiates functional domains of the skeleton, Bioconjug. Chem. 18 (5) (2007) 1375–1378.
[148] J. Liu, Y. Zeng, S. Shi, L. Xu, H. Zhang, J.L. Pathak, Y. Pan, Design of polyaspartic acid peptide-poly (ethylene glycol)-poly (ε-caprolactone) nanoparticles as a carrier of hydrophobic drugs targeting cancer metastasized to bone, Int. J. Nanomedicine 12 (2017) 3561.
[149] Y. Wu, Y. Yang, W. Zhao, Z.P. Xu, P.J. Little, A.K. Whittaker, R. Zhang, H.T. Ta, Novel iron oxide–cerium oxide core–shell nanoparticles as a potential theranostic material for ROS related inflammatory diseases, J. Mater. Chem. B 6 (30) (2018) 4937–4951.
[150] H.T. Ta, N. Arndt, Y. Wu, H.J. Lim, S. Landeen, R. Zhang, D. Kamato, P.J. Little, A. K. Whittaker, Z.P. Xu, Activatable magnetic resonance nanosensor as a potential imaging agent for detecting and discriminating thrombosis, Nanoscale 10 (31) (2018) 15103–15115.
[151] K.X. Vazquez-Prada, J. Lam, D. Kamato, Z.P. Xu, P.J. Little, H.T. Ta, Targeted molecular imaging of cardiovascular diseases by iron oxide nanoparticles, Arteriosclerosis, Thrombosis, and Vascular, Biology 41 (2) (2021) 601–613.
[152] A. Zia, Y. Wu, T. Nguyen, X. Wang, K. Peter, H.T. Ta, The choice of targets and ligands for site-specific delivery of nanomedicine to atherosclerosis, Cardiovasc. Res. 116 (13) (2020) 2055–2068.
[153] Y. Liu, Y. Wu, R. Zhang, J. Lam, J.C. Ng, Z.P. Xu, L. Li, H.T. Ta, Investigating the use of layered double hydroxide nanoparticles as carriers of metal oxides for theranostics of ROS-related diseases, ACS Appl. Bio Mater. 2 (12) (2019) 5930–5940.
[154] Y. Zhang, A. Koradia, D. Kamato, A. Popat, P.J. Little, H.T. Ta, Treatment of atherosclerotic plaque: perspectives on theranostics, Journal of Pharmacy and Pharmacology 71 (7) (2019) 1029–1043.
[155] H.T. Ta, S. Prabhu, E. Leitner, F. Jia, K. Putnam, N. Bassler, K. Peter, C.J.C. R. Hagemeyer, Antibody-sortagging: a universal approach towards targeted molecular imaging and cell homing in cardiovascular disease, Circ. Res. 107 (12) (2010) e37–e38.
[156] S. Adirekkiat, V. Sumethkul, A. Ingsathit, S. Domrongkitchaiporn, B. Phakdeekitcharoen, S. Kantachuvesiri, C. Kitiyakara, P. Klyprayong, S. Disthabanchong, Sodium thiosulfate delays the progression of coronary artery calcification in haemodialysis patients, Nephrology Dialysis Transplantation 25 (6) (2010) 1923–1929.
[157] A.U. Rehman, Y. Wu, H.D. Tran, K. Vazquez-Prada, Y. Liu, H. Adelnia, N. D. Kurniawan, M.N. Anjum, S.S. Moonshi, H.T. Ta, Silver/iron oxide nano-popcorns for imaging and therapy, ACS Appl. Nano Mater. 4 (10) (2021) 10136–10147.
[158] Y. Wu, K.X. Vazquez-Prada, Y. Liu, A.K. Whittaker, R. Zhang, H.T. Ta, Recent advances in the development of theranostic nanoparticles for cardiovascular diseases, Nanotheranostics 5 (4) (2021) 499.
[159] S.S. Moonshi, Y. Wu, H.T. Ta, Visualizing stem cells in vivo using magnetic resonance imaging, Wiley Interdiscip. Rev. Nanomed. Nanobiotechnol. 14 (2) (2022), e1760.
[160] Y. Wu, G. Cowin, S.S. Moonshi, H.D. Tran, N.A. Fithri, A.K. Whittaker, R. Zhang, H.T. Ta, Engineering chitosan nano-cocktail containing iron oxide and ceria: A two-in-one approach for treatment of inflammatory diseases and tracking of material delivery, Mater. Sci. Eng. C 131 (2021), 112477.
[161] N.N.M. Yusof, A. McCann, P.J. Little, H.T. Ta, Non-invasive imaging techniques for the differentiation of acute and chronic thrombosis, Thromb. Res. 177 (2019) 161–171.
[162] H.T. Ta, Z. Li, Y. Wu, G. Cowin, S. Zhang, A. Yago, A.K. Whittaker, Z.P. Xu, Effects of magnetic field strength and particle aggregation on relaxivity of ultra-small dual contrast iron oxide nanoparticles, Mater. Res. Express 4 (11) (2017), 116105.
[163] H.T. Ta, S. Prabhu, E. Leitner, F. Jia, D. von Elverfeldt, K.E. Jackson, T. Heidt, A. K.N. Nair, H. Pearce, C. Von Zur Muhlen, Enzymatic single-chain antibody tagging: a universal approach to targeted molecular imaging and cell homing in cardiovascular disease, Circ. Res. 109 (4) (2011) 365–373.
[164] H.T. Ta, Z. Li, C.E. Hagemeyer, G. Cowin, S. Zhang, J. Palasubramaniam, K. Alt, X. Wang, K. Peter, A.K. Whittaker, Molecular imaging of activated platelets via antibody-targeted ultra-small iron oxide nanoparticles displaying unique dual MRI contrast, Biomaterials 134 (2017) 31–42.
[165] T. Cowger, J. Xie, Polyaspartic acid coated iron oxide nanoprobes for PET/MRI imaging, in: Nanomaterial Interfaces in Biology, Springer, 2013, pp. 225–235.
[166] S. Marasini, H. Yue, A. Ghazanfari, S.L. Ho, J. Park, S. Kim, H. Cha, S. Liu, T. Tegafaw, M.Y. Ahmad, Polyaspartic acid-coated paramagnetic gadolinium oxide nanoparticles as a dual-modal T1 and T2 magnetic resonance imaging contrast agent, Appl. Sci. 11 (17) (2021) 8222.
[167] T. Veres, C. Voniatis, K. Molnár, D. Nesztor, D. Fehér, A. Ferencz, I. Gresits, G. Thuróczy, B.G. Márkus, F. Simon, An implantable magneto-responsive poly (aspartamide) based electrospun scaffold for hyperthermia treatment, Nanomaterials 12 (9) (2022) 1476.
[168] A. Jedlovszky-Hajdu, K. Molnar, P.M. Nagy, K. Sinko, M. Zrinyi, Preparation and properties of a magnetic field responsive three-dimensional electrospun polymer scaffold, Colloids Surf. A Physicochem. Eng. Asp. 503 (2016) 79–87.
[169] H. Huang, T. Yue, K. Xu, J. Golzarian, J. Yu, J. Huang, Fabrication and evaluation of tumor-targeted positive MRI contrast agent based on ultrasmall MnO nanoparticles, Colloids Surf. B: Biointerfaces 131 (2015) 148–154.
[170] M. Kumagai, M.R. Kano, Y. Morishita, M. Ota, Y. Imai, N. Nishiyama, M. Sekino, S. Ueno, K. Miyazono, K. Kataoka, Enhanced magnetic resonance imaging of

experimental pancreatic tumor in vivo by block copolymer-coated magnetite nanoparticles with TGF-β inhibitor, J. Control. Release 140 (3) (2009) 306–311.
[171] M. Kumagai, Y. Imai, T. Nakamura, Y. Yamasaki, M. Sekino, S. Ueno, K. Hanaoka, K. Kikuchi, T. Nagano, E. Kaneko, Iron hydroxide nanoparticles coated with poly (ethylene glycol)-poly (aspartic acid) block copolymer as novel magnetic resonance contrast agents for in vivo cancer imaging, Colloids Surf. B: Biointerfaces 56 (1–2) (2007) 174–181.
[172] J. Feng, L. Gao, R. Wen, Y. Deng, X. Wu, S. Deng, Fluorescent polyaspartic acid with an enhanced inhibition performance against calcium phosphate, Desalination 345 (2014) 72–76.
[173] S. Palaniappan, M.S. Ram, Esterification of carboxylic acids with alcohols catalyzed by polyaniline salts, Green Chem. 4 (1) (2002) 53–55.
[174] J. MacAdam, P. Jarvis, Water-formed scales and deposits: types, characteristics, and relevant industries, in: Mineral Scales and Deposits, Elsevier, 2015, pp. 3–23.
[175] D. Bazin, C. Leroy, F. Tielens, C. Bonhomme, L. Bonhomme-Coury, F. Damay, D. Le Denmat, J. Sadoine, J. Rode, V. Frochot, E. Letavernier, J.-P. Haymann, M. Daudon, Hyperoxaluria is related to whewellite and hypercalciuria to weddellite: what happens when crystalline conversion occurs? C. R. Chim. 19 (11) (2016) 1492–1503.